Growth and structural characterization of GaP/Ga($P_{1-x}Sb_x$) nanowires

LUNDS UNIVERSITET

Lunds Tekniska Högskola

Dario Stjärnemyr Ghidini

Acknowledgements

During this project and my time at LTH there are people who have supported and inspired me. First I would like to thank my supervisor Kimberly Dick Thelander, a great inspiration whom have taught me a great deal about electron microscopy, epitaxial growth and III-V materials and always found time to discuss my ideas. Sepideh Gorji Ghalamestani, Daniel Jacobsson and Sebastian Lehmann, three amazing people who helped me out and taught me the practical parts and whom were always open to talk and share their knowledge. Thank you, you really made me feel like a part of the group. Outside of the group there are people who I would like to thank as well, Jonas Johansson whom together with Kimberly inspired me to go into material science and physics. Crispin Hetherington, Martin Ek and Filip Lenrick for teaching me new things and helping out on the TEM. Gunnel Karlsson for keeping the TEM running and the NanoLab staff for keeping the lab running. Last I would like to thank Knut Deppert, Elisabeth Nilsson and Lars Samuelson for their involvement in starting and running the "Engineering Nanoscience" education program.

Abstract

In this thesis epitaxial growth of $Ga(P_{1-x}Sb_x)$ and analysis by electron microscopy are presented. To the authors knowledge $Ga(P_{1-x}Sb_x)$has not been grown in the form of nanowires before and the main motivation of this work is to investigate the possibility of overcoming the miscibility gap (1-99%) in nanostructures [1-4]. The goal of this project is to gain a better understanding of the general behavior of Sb-based materials (precursors) in Metal-Organic Vapor Phase Epitaxy (MOVPE) growth system and its influence on the growth of Sb-containing compounds. Our findings can be used to improve the understanding of growth and enhance the level of control of other Sb-containing binary and ternary material systems. The nanowires were analyzed by both Scanning Electron Microscopy (SEM) and Transmission Electron Microscopy (TEM). In order to get chemical composition, X-ray Energy Dispersive Spectroscopy (EDS) was performed in combination with TEM.

The results of the growth experiments indicate that the incorporation of Sb into a GaP-based matrix is limited when attempting the growth of ternary nanowires grown on a GaP stem. Within this study, the growth conditions of the experiments were pushed towards the technical limit of the machine setup (the molar flows were maximized and minimized, respectively) and we found indications that successful growth of ternary $Ga(P_{1-x}Sb_x)$ nanostructures with variable Sb content $0<x<1$ might take place at even more extreme conditions. The presence of Sb-based species in the growth system has induced up to 90% reduction of the growth rate of the nanowires and it is likely due to Sbs surfactant and surface wetting properties. Further, the growths of $Ga(P_{1-x}Sb_x)$ performed with a ratio between P and Sb molar fractions lower than 2:1 have shown deviations from the standardly found Au_xGa_{1-x} particle composition and resulted in the formation of a two-phased particle with a second gold phase-$AuSb_2$. This project has shown previously unknown properties of Sb and Sb-containing ternaries and has opened up the material system for further investigations.

Popular science summary

The demands for new and better products by the consumers create challenges for development of future technology. Nanotechnology has the potential to be the answer to the challenges and is today a hot topic but in reality it is a subject that has been studied for decades. Products containing nanotechnology exist on the market today such as self-cleaning windows and stainless clothing. More advanced applications are being researched such as light emitting diodes (LEDs), solar cells and other advanced electronic devices. To develop a good product containing nanotechnology precise control and the ability to tailor structures and materials are required.

What is nano? It is the collective word for structures and materials that have been shrunk down to the nanoscale. The nanoscale is usually defined as the size between 0,1 and 100 nanometers (1 nanometer = 0,000 000 001 meter) e g sizes more than 1000 times smaller than the thickness of a human hair.

To develop and tailor new materials, small amount of materials with known properties are combined to get new exciting and useful properties. To get a better understanding of what this mean imagine trying to mix a unique color shade, you have the different pure colors and depending on how and how much of each color you use, the color shade you are creating will change, too much of one of the pure colors and it will no longer become the shade of color you were after, you need to get the right amount of each of the pure colors.

In modern semiconductor technology, components are made out of silicon (Si). Silicon technology is well developed and the material cost is low resulting in cheap components. Silicon technology does however suffer from some limitations which can be avoided by using other kinds of semiconductor materials. By combining elements from group III (3) and group V (5) in the periodic table (see figure 1), semiconductor materials with better performance, lower energy consumption and new properties can be achieved. III-V materials are more expensive than silicon and therefore there is an interest in combining III-V materials with existing silicon semiconductor technology to take advantage of the best of both worlds.

						1 H 1.00794	2 He 4.002602
		5 B 10.811	6 C 12.0107	7 N 14.00674	8 O 15.9994	9 F 18.9984032	10 Ne 20.1797
		13 Al 26.981538	14 Si 28.0855	15 P 30.973761	16 S 32.066	17 Cl 35.4527	18 Ar 39.948
29 Cu 63.546	30 Zn 65.39	31 Ga 69.723	32 Ge 72.61	33 As 74.92160	34 Se 78.96	35 Br 79.904	36 Kr 83.80
47 Ag 107.8682	48 Cd 112.411	49 In 114.818	50 Sn 118.710	51 Sb 121.760	52 Te 127.60	53 I 126.90447	54 Xe 131.29
79 Au 196.96655	80 Hg 200.59	81 Tl 204.3833	82 Pb 207.2	83 Bi 208.98038	84 Po (209)	85 At (210)	86 Rn (222)

Figure 1. Part of the periodic table. Highlighted in green are the most common group III elements used. The yellow are the commonly used group V elements.

Modern components are created by what is referred to as a “top-down” method. “Top-down” method can be explained by imagining a large stone block where you chisel away parts and polish it to get the desired shape. The opposite to this is the “bottom-up” method, where instead of removing you start with an empty surface and stack piece on top of each other to obtain the desired shape. The advantage with the “bottom-up” method is that small structures can be made faster and in a more controlled manner. In this project a “bottom-up” method known as MOCVD was employed the build structures called nanowires. In a MOCVD machine pressure, temperature and amount of reacting materials (stacking pieces) can be controlled. Nanowires are grown “atom-by-atom” and in this project they were grown from a small gold particle called a “seed” particle. Nanowires can be described as one dimensional rod-shaped structures (see figure 2). They are characterized as having a large “length-to-width” ratio meaning their diameter ranges from a few, to tens of nanometers and their length is typically of the order of a few micrometers (0,000 001 meter).

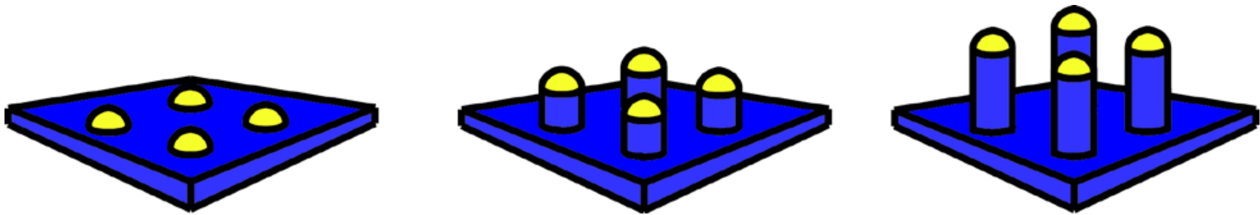

Figure 2. Schematic illustration of nanowire growth. The left image shows the gold particles on an open surface. The middle and the right image show different stages of grown nanowires.

Antimonides are exciting materials for future semiconductor technology with great potential for high-speed electronics with lower energy consumption than conventional silicon based electronics. In this project, gallium phosphide antimonide (GaPSb) has been studied, with a goal of gaining a better understanding of antimony containing semiconductor materials.

We have investigated how the amount of each different reacting materials, gallium, phosphor and antimony, affect the finished product (GaPSb nanowires). By using advanced microscopy we have investigated how the reacting materials affect the length of the finished nanowires. Our experimental setup has been to keep the amount of two materials constant while varying the third one. Following the concept of mixing colors, we have mixed green (GaP) and purple (GaSb) to get different shades of brown (GaPSb), by changing the amount of red (P), blue (Sb) and yellow (Ga) used to mix the purple and the green. We have shown that the length is dependent on the amount of gallium by becoming longer if the amount of gallium we use is increased. The opposite have been seen when antimony is increased, the nanowires become shorter as the amount of antimony is increased. For phosphor we have not seen any dependence on the amount but rather a constant length when phosphor was changed.

The composition or how much antimony that could be introduced into the gallium phosphide nanowires was also investigated. By using x-rays from the material generated by adding energy to the material it is possible to determine what elementals and how much of each element there is in a nanowire. We have found a variation between 1 and 7 % antimony and the corresponding amount of phosphor is then 99 to 93 %. In summary, this project has shown the first successful and important steps in understanding gallium phosphide antimonide and antimony containing semiconductor materials.

Abbreviations

at%	Atomic percent
BSE	Backscatter Electron
EDS (XEDS)	X-ray Energy Dispersive Spectroscopy
Ga	Gallium
HAADF	High-Angle Annular Dark Field
HR-TEM	High-Resolution Transmission Electron Microscopy
In	Indium
m.f.	Molar fraction
MOVPE	Metal-Organic Vapor Phase Epitaxy
PH_3	Phosphine
Sb	Antimony
SE	Secondary Electron
SEM	Scanning Electron Microscopy
STEM	Scanning Transmission Electron Microscopy
(c)TEM	conventional Transmission Electron Microscopy
TMGa	Trimethylgallium
TMSb	Trimethylantimony
WZ	Wurtzite
ZB	Zinc-blende

Contents

Acknowledgements ... I
Abstract ... II
Popular science summary ... III
Abbreviations ... V
Chapter 1 ... 1
Introduction – A reason for ternaries and antimonides ... 1
1.1 Nanotechnology ... 1
1.2 Antimonides ... 2
Chapter 2 ... 3
Epitaxial growth ... 3
2.1 Crystals ... 3
2.2 Epitaxy ... 3
2.3 Thermodynamics of epitaxial growth ... 5
2.4 Metal-organic vapor phase epitaxy (MOVPE) ... 6
2.5 Metal-particle assisted epitaxial nanowire growth ... 7
2.6 Growth of heterostructures ... 8
2.7 Molar fraction and V/III ratio ... 9
Chapter 3 ... 11
Electron microscopy ... 11
3.1 Scanning Electron Microscopy (SEM) ... 13
3.2 Transmission Electron Microscopy (TEM) ... 14
3.3 Analytical Electron Microscopy and X-ray Energy-Dispersive Spectroscopy (EDS) ... 16
Chapter 4 ... 17
Gallium phosphide antimonide ... 17
4.1 Lattice mismatch ... 17
4.2 Surfactant effect ... 18
4.3 Growth series, effects and limitations ... 19
4.3.1 Gallium growth series ... 19
4.3.2 Phosphor growth series ... 20
4.3.3 Antimony growth series ... 21
4.4 Growth challenges ... 21
4.5 Seed particle and Crystal structure ... 25
Chapter 5 ... 28
Conclusions ... 28
5.1 Outlook ... 28
Appendix A ... 30
Growth parameters ... 30
Appendix B ... 35
EDS results ... 35
References ... 40

Chapter 1

Introduction – A reason for ternaries and antimonides

1.1 Nanotechnology

The world of nanotechnology is today on everyone's lips but in reality it is a subject that has been studied for decades. Products containing nanotechnology exist on the market today such as self-cleaning windows and clothing that doesn't get stained. More advanced applications are being researched such as light emitting diodes (LEDs), solar cells and other electronic devices. To develop a good product containing nanotechnology require us to have precise control and the ability to tailor structures to our needs.

For more than a decade the research in Lund has been focused on controlling and understanding the mechanisms of binary systems in both homo- and heterostructure. The limitations of binary systems is their inflexibility, a binary system has one lattice parameter, one bandgap, one set of properties. To tailor a product for the needs of tomorrow, flexibility is required and ternaries provide the ability. In short a ternary system is a mixture of two binary systems and by controlling the mixture, any bandgap and lattice parameter between the two binaries can be obtained, while allowing the ternary to have its own unique properties. However, ternaries are a double edged blade, the increased flexibility entail an increase in parameters that require control, e.g. material A no longer only affects material B, A affects material C and can affect how B and C affect each other. It becomes complicated very fast. For this reason many ternary combinations are poorly studied even when the benefits overweigh the challenges faced in growing them.

Nanowires grown "atom-by-atom" are one dimensional rod-shaped structures, they are characterized by having a large "length-to-width" ratio, their diameter ranges from a few, to tens of nanometers and their length is typically of the order of a few micrometers. Nanowires have unique properties e.g. surface-related effects, crystal structure effects and strain-relaxation effects. Surface-related effects arise from the large "surface-to-volume" ratio of nanowires. The crystal structure and defect ratio of the growing material can be highly controlled by the growth parameters and contribute to nanowires unique properties. There are some properties that are uniquely achievable in nanowires, such as defect free materials in highly lattice mismatched materials, these properties can however be achieved in nanowires by their unique lateral strain relaxation. Growing nanowires "atom-by-atom" gives the freedom to engineer materials the way we need them.

Nanowire structures can be produced by metal-organic vapor phase epitaxy (MOVPE), a relatively fast, flexible and reliable method with a large range of available material sources. Considering the scale on which epitaxial growth takes place, the system is equivalent to a "black box". A small change is made to an input parameter and then the results are observed, a trial-and-error procedure. Any growth study begins with seemingly random attempts to obtain a starting point based on prior experience and understanding of similar material systems and then branch out from there. Each growth gives you one more puzzle piece to understanding your material system.

1.2 Antimonides

Sb containing III-V materials are interesting for fundamental physics and electronic applications. At this point, Sbs are underdeveloped in nanowire growth compared to the conventional arsenide, phosphide and nitride materials due to the significant differences in material properties and growth behavior. Ternary Sbs are particularly interesting, since many of these materials have important infrared bandgaps and several cannot be easily fabricated in bulk, or layers due to the large difference in growth conditions. $Ga(P_{1-x}Sb_x)$ is one example of these ternary Sbs and is an important and a remarkable material system which is extremely hard to mix due to its poor miscibility and that the high growth temperatures typically used to grow GaP layers (700-850°C) [5] are incompatible with the low melting point of GaSb (712°C). Further the investigation of $Ga(P_{1-x}Sb_x)$ is interesting to experimentally establish at what composition the bandgap changes from, indirect (GaP) to direct (GaSb) with a transition calculated to occur at around 35% Sb but no experimental data is available to confirm it.

By using the properties of MOVPE together with the unique properties of nanowires it may be possible to achieve compositions, not easily obtainable due to the poor miscibility and that is worth investigating. The main motivation of this project was to investigate the possibility of overcoming the miscibility gap in nanostructures and to gain a better understanding of the general behavior of Sb-based materials (precursors) in Metal-Organic Vapor Phase Epitaxy (MOVPE) growth system and its influence on the growth of Sb-containing compounds. This would provide valuable information that can be used to improve the level of control for growth of other Sb-containing materials.

Chapter 2

Epitaxial growth

2.1 Crystals

A unit cell is the smallest repeating part of a crystal and by translating the unit cell along all crystallographic directions a crystal is formed. This means that each unit cell is surrounded by other identical unit cells.

III-V materials crystallize in either zinc-blende (ZB) or wurtzite (WZ) crystal structure. Atoms in ZB and WZ structure bind to each other with four hybridized sp^3 electron orbitals. sp^3 orbitals form very strong and directional covalent bonds arranged into the corners of a tetrahedron. The extra electron present in the group-V species transfers to the group-III specie to form a slightly ionic bond between the sp^3 orbitals of the two species [6 and refs within]. Along the [111] axis the atomic bilayers in ZB have the cubic stacking sequence ABCABC while WZ in the equivalent hexagonal [0001] have the stacking sequence of ABABAB, shown in figure 2.1 with the additional notation to describe the single layers, AaBbCc and AaBbAa.

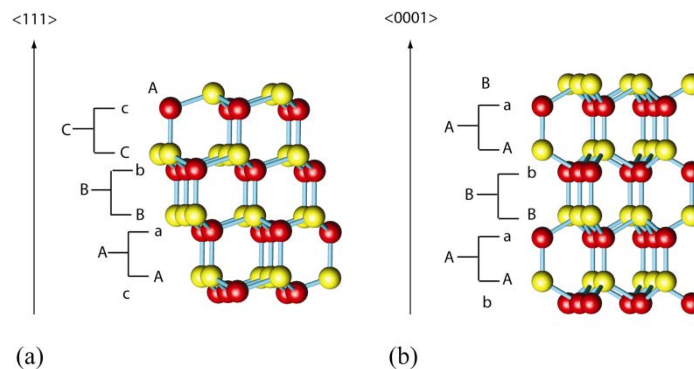

Figure 2.1 Atomic structures (a) for ZB crystal and (b) for the WZ crystal. Both models are slightly rotated from the ⟨1 1 0⟩ viewing direction. The different colors for the atoms represent the two types of atoms (group III and V) [7]. With permission from Jessica Bolinsson, PhD.

2.2 Epitaxy

Epitaxy comes from the Greek words *epi* (meaning "on") and *taxis* (meaning "ordered arrangement"). It can be described as the ordered growth of crystalline material on a substrate. The crystal orientation of the substrate is adopted by the grown material. It is a chemical reaction which is governed by the materials phase diagram and the growing material will strive to reach equilibrium, the lowest total energy configuration. By supersaturating the reaction with educt species the reaction is pushed to form the product in a constant attempt to move towards equilibrium.

If the deposited material is identical to the substrate the growth is referred to as homoepitaxy, from the Greek word *homos* (meaning “same”). Should the grown material be different than the substrate then it is referred to as heteroepitaxy, from the Greek word *heteros* (meaning “different”).

Epitaxially grown III-V semiconductor structures are prepared by using at least one group III and one group V material. A III-V binary system is formed if one element of each group is used, for example Ga and P form the binary III-V material GaP. Most epitaxial growth in research today is done on binary systems but ternaries are becoming increasingly interesting for the increased flexibility of their electronic band structure and lattice parameter. A ternary is a system where a second group III or group V element is introduced to the growth, a III-III-V or III-V-V system and can be described as a mix of two binaries. The band structure of the ternary system is governed by an extension of Vegard’s law which states that the bandgap is a function of the ratio between the two binary systems and the bowing parameter b [8]

$$E_{g(Ga(P1\text{-}xSbx))} = xE_{g(GaSb)} + (1\text{-}x)E_{g(GaP)} - bx(1\text{-}x) \qquad (2.1)$$

where x is the amount of GaSb in this case. The bowing parameter is in general experimentally determined for systems and then theoretical calculations are made to fill in the gaps. In figure 2.2 II-VI and III-V material combinations with their estimated transitions between direct and indirect bandgaps are shown.

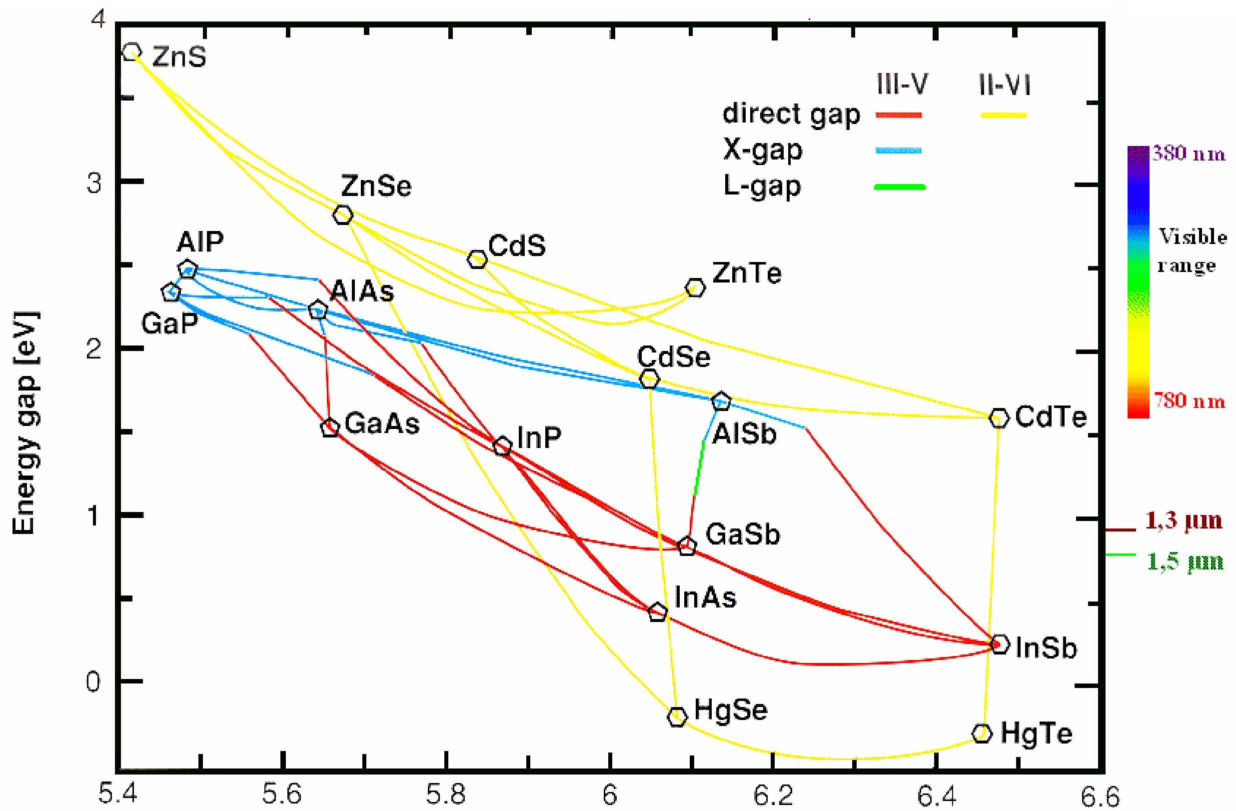

Figure 2.2 Energy gap of different material systems plotted versus their lattice parameters calculated by Vegard’s law.

2.3 Thermodynamics of epitaxial growth

During epitaxial growth the system tries to reach equilibrium, the lowest energy phase of the system. The driving force to achieve equilibrium is the difference in chemical potential ($\Delta\mu$) between the different phases in the system. If there are two states, A and B then difference would be expressed as:

$$\Delta\mu = \mu_A - \mu_B \qquad (2.2)$$

$\Delta\mu$ is a measurement of the supersaturation of the system and at equilibrium the chemical potential, $\Delta\mu$ is equal to zero (i.e. $\mu_A = \mu_B$). The chemical potential for a given phase, μ_i, is a measurement of the change in Gibbs free energy, G, at an infinitesimal change in amount of material, n_i, for this phase at constant temperature and pressure:

$$\mu_i = \left(\frac{\delta G}{\delta n_i}\right)_{T,P,n_j} \qquad (2.3)$$

If the system is in non-equilibrium it will go from the high towards the low chemical potential to restore equilibrium. If A is the condensed phase and B is the vapor phase a supersaturation ($\Delta\mu$) in the vapor phase will force the system into the condensed phase. The phase transition will occur at the surface of the condensed phase and in particle seeded nanowire crystalline structures it will result in epitaxial growth at the interface between the seed particle and the top of existing crystal.

In epitaxial growth performed by MOVPE the supplied sources and the material in the epitaxial layers are not the same, the supplied sources are generally precursor molecules containing the desired atoms. Before the supplied sources can be incorporated into the epitaxial layer they must be *decomposed* or *cracked* by pyrolytic reactions. This means that a number of reactions governed by kinetics are required before growth can occur. For the bonds in the molecules to break by pyrolysis, the surrounding needs to supply enough energy e g through heat. If the temperature is too low no or only a fraction of the molecules will decompose which may result in a growth rate limiting step. Low growth temperature may also result in impurities being incorporated into the growing layer as a result of incomplete decomposition. When the temperature is raised to a level sufficient enough to assure complete decomposition of the source material then the growth rate will be limited by the mass transport or the diffusion of the atoms. In this temperature region the growth rate is mostly independent of the temperature and relies solely on the speed with which material is being supplied to the growth location.

When growth is limited by kinetics there is a reaction step that limits the rate of growth. The rate of growth (k) then depends on two factors, temperature of the system (T) and the activation energy (E*) associated with the limiting reaction step. The activation energy is a barrier which the reaction step needs to overcome to take place. The rate of reaction/growth can be expressed as the Arrhenius equation;

$$k = Ae^{-E^*/RT} \qquad (2.4)$$

where A is referred to as the pre-exponential factor and depends on the type of reaction step. For a first order reaction A has units of s^{-1}. If several reactions or reaction steps are present then the step with highest activation energy will determine the overall rate, much like a bottle neck.

Should the reaction take place in the diffusion limited regime then the rate of growth is limited by how fast new material can be supplied to the growth interface. What this implies is that the growth interface consumes the material faster than new material can be supplied to the interface. Film growth normally takes place in this regime while nanowire growth often is performed in the kinetically limited regime. [9, 10] [11, 12 and refs within]

2.4 Metal-organic vapor phase epitaxy (MOVPE)

There are several methods for epitaxial growth and during this project metal-organic vapor phase epitaxy (MOVPE) was employed to grow nanowires. MOVPE can be operated from atmospheric pressure (1013 mbar) to low pressure (10 mbar) and the latter is referred to as low-pressure (LP)-MOVPE. During this project a reactor pressure of 100 mbar was used during growth. In MOVPE at least one source is a metal-organic compound, typically the group III source for III-V material growth. The metal-organic sources are situated in containers called bubblers which are kept in temperature controlled baths. The metal-organic sources are mostly in liquid form (e.g. trimethylgallium, TMGa) but a few are found in solid form (e.g. trimethylindium, TMIn). An ultra-pure inert carrier gas, typically hydrogen (H_2) is transported to the bubbler and released below the liquid level. The inert carrier gas is bubbled through the metal-organic liquid and the vapor pressure of the metal-organic and the total pressure of the bubbler is preserved by transporting the bubbles away from the bubbler to the reactor during growth. An electronic-pressure controller (EPC) measures and controls the pressure in the bubbler while a mass-flow controller (MFC) adjusts the flow of the inert carrier gas to keep a constant flow in the system. Group V sources like phosphorous (P) and arsenic (As) are typically found in stable gaseous hydride form (e.g. phosphine, PH_3 and arsine, AsH_3) and are kept in gas bottles. In this project the phosphine did not require a carrier gas and are sent directly to the reactor while the antimony (Sb) source employed was the metal-organic trimethylantimony (TMSb), due to having no stable hydride. [11, 12, 13 and refs within] Figure 2.3 show an illustration of the system and sources used for this project.

During growth the substrate is placed on a graphite susceptor situated inside the reactor. The susceptor rotates to assure a laminar flow of sources for a homogeneous deposition of material over the substrate. Sources are only transported to the reactor when growth is desired at all other times they are flushed out to be either burned or filtered by what is called a scrubber to render them harmless, the same is done with any growth material and rest products that has not incorporated into the sample. The control for this is achieved by the Vent/Run system. To stimulate growth heat is required and the susceptor is heated either by radio-frequencies or by infra-red light.

In practice when using MOVPE there are several factors which can limit or improve the rate of growth, incorporation and crystal structure. Factors like relative concentration of source material, pressure in the reactor and gas flow speed. Typically the presence of hydrogen (H_2) enhances the decomposition and is therefore the commonly used carrier gas. In addition the precursor decomposition can also be improved

when both hydride and metal-organic sources are present. However, in the presence of hydrogen (H_2) metal-organic precursors generally decompose at a lower temperature than hydrides which can result in decomposition of the metal-organic precursor before it can enhance the decomposition of the hydride precursors at a given temperature. The substrate surface can affect decomposition and growth. [9, 14-17]

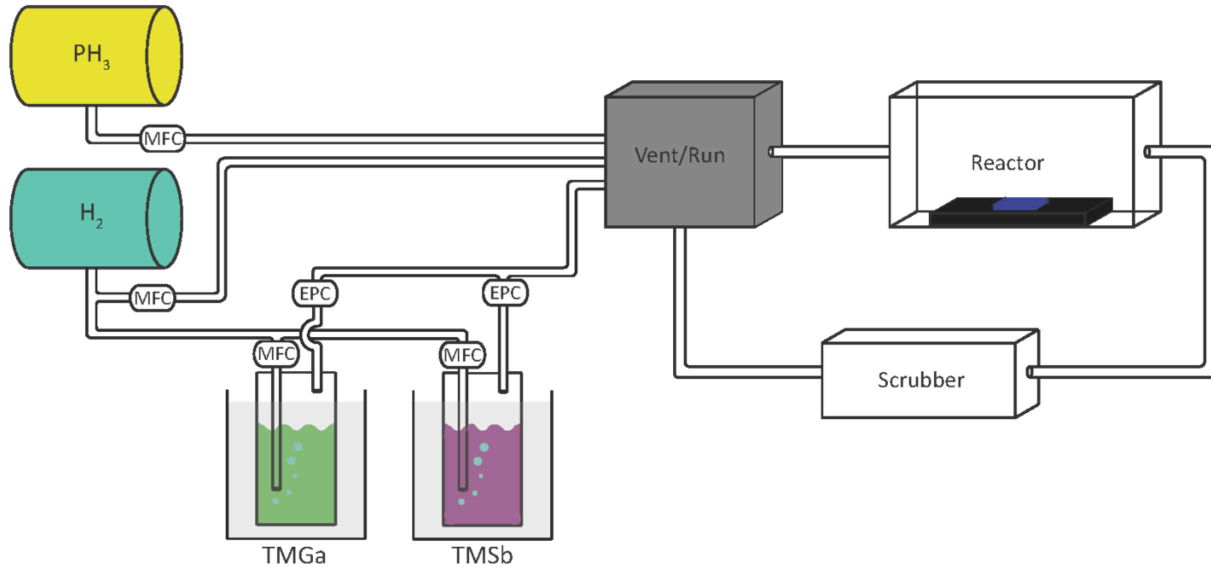

Figure 2.3 Overview illustration of MOVPE machine and the sources employed in this project.

2.5 Metal-particle assisted epitaxial nanowire growth

To grow nanowires growth must in the general case be promoted in some locations. This can be achieved with the help of seed particles, which can be made and defined on the substrate by several techniques; evaporation and condensation, electron beam lithography (EBL), annealing of a thin film deposited on the substrate or by deposition of colloidal particles. The seed particle material varies; typically Au or the metal of the desired growth material is used, such as group III for III-V materials.

The first step is to deposit the seed particles. Normally this is done on the (111)B surface of the substrate; it is the most commonly used for the growth of nanowires. During this project Au seed particles were defined on the substrates by evaporating Au, letting it condense in the vapor phase and last deposit it onto the substrate as shown in figure 2.4 b).

After deposition the substrate is transferred to the MOVPE reactor cell where it is annealed at relatively high temperature (600-800°C) for 5-15 min to remove any native oxides; this is done under group V pressure to prevent the substrate from decomposing. After annealing the temperature is set to the desired growth temperature and the group III source is added to the reactor. The seed particle can alloy with the group III element in the substrate during annealing or with the group III source when it is added to the reactor. Figure 2.4 c) illustrate the alloying of the gold particle and the overpressure of group V precursor associated with annealing. As more material is transported to the reactor the seed particle will

supersaturate and precipitate III-V material at the interface between the substrate and the seed particle. Later the precipitation will occur at the interface between the already grown nanowire and the seed particle (d) and e)). Growth will take place while enough source material is present in the reactor to precipitate material.

It is usually desired to have seed particles of a specific diameter and with a known surface density since it determines the diameter and surface density of the nanowires and helps to make reproducible results. For this project each growth consisted of two substrates, one with 50 nm Au particles and one with multiple diameter particles (20, 40, 50, 60, 80 nm) both substrates had a total density of 1 μm^{-2} (0.2 μm^{-2} per particle size on multiple diameter substrate).

2.6 Growth of heterostructures

Heterostructures are not only limited to the epitaxially grown material being different than the substrate, it also includes having different materials in a single nanowire . The change in material can either be along the nanowire growth direction, referred to as axial heterostructure (figure 2.4 f)) or around the nanowire, so called radial heterostructure or core-shell structure. Heterostructures can be achieved by changing or adding group III and/or group V sources during the growth. Different temperatures promote axial and radial growth differently and it is difficult to find a region where one is promoted and the other suppressed. Axial growth is generally desired and some radial overgrowth usually takes place on the sides of the nanowire resulting in nanowires being wider at the base than the top termed tapering. Typically higher temperature results in higher radial growth rates then observed at lower temperatures [18, 19].

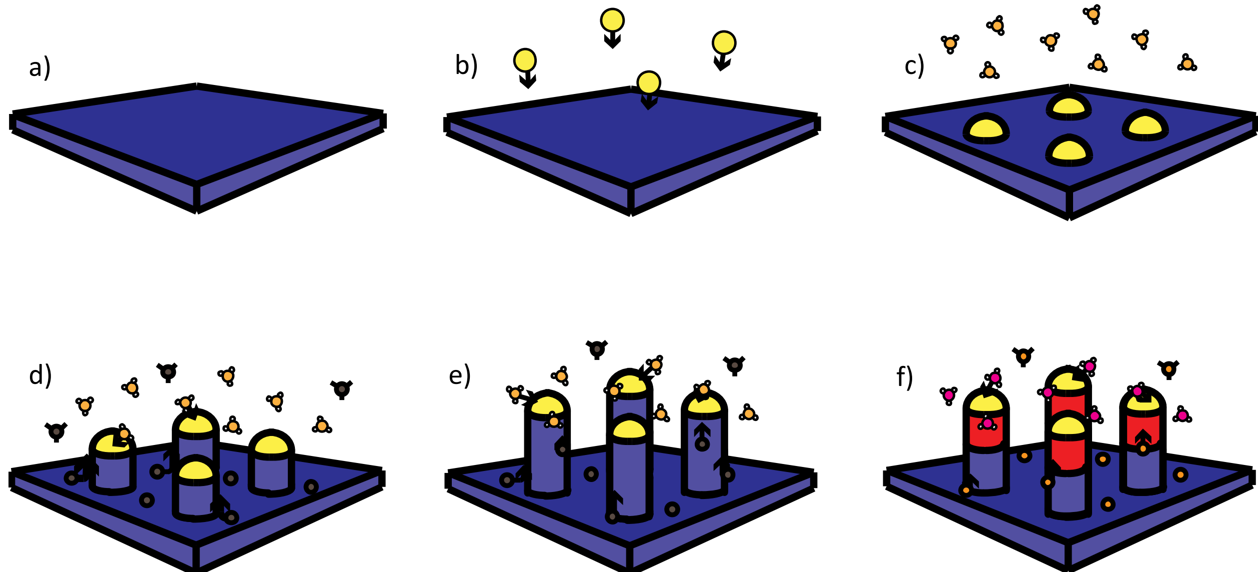

Figure 2.4 Schematic illustration of Au assisted particle growth with precursor and surface diffusing species. (a) substrate, (b) deposition of Au particles on to the substrate, (c) annealing and alloying of particle, (d) initial growth, (e) nanowire growth and (f) growth of a heterostructure.

When growing a heterostructure it can be important to create an abrupt interface between the two different segments of the nanowire and the abruptness can often be achieved with a rapid switch between the sources but it is also dependent on which order the materials are grown. Certain material combination can only create unidirectional abrupt-interfaces, for example A on B may grow but not B on A [20].

2.7 Molar fraction and V/III ratio

In papers on epitaxial growth performed with MOVPE two factors are commonly used to link results with parameter settings, these are called the molar fraction and the nominal input value of the V/III ratio. To understand their effect, it is important to understand what they are. For metal-organic materials the molar fraction χ_i for material i is the ratio of the source flow from the bubbler of the metal-organic material ($q_{i,bubbler}$) compared to the total flow in the reactor (Q_{tot}) (eq. 2.5).

$$\chi_i = \frac{P_{i,partial}\ (Pa) * q_{i,bubbler}(\frac{m^3}{s})}{Q_{tot}(\frac{m^3}{s}) * P_{i,bubbler}(Pa)} \tag{2.5}$$

where $P_{i,partial}$ is the partial pressure of the metal-organic material i and $P_{i,bubbler}$ is the total pressure in the bubbler of metal-organic material i.

The molar fraction of hydride material in MOVPE is a lot simpler to calculate than the molar fraction of the metal-organic material due to not requiring a carrier gas to reach the reactor. Instead the molar fractions of the hydrides depend on the machine system and the calibration of the MFCs in the machine setup according to eq. 2.6;

$$\chi_i = \frac{q_i}{Q_{tot}} * C \tag{2.6}$$

here C is the calibration constant of MFC in the system.

When growing III-V materials an equal part group III and group V material is consumed but how accessible these materials are, depend on the thermodynamics of the system. To make sure there is sufficient material to promote growth a surplus of one material is commonly used, normally group V for nanowire growth since hydrides rarely stick to the surface and gets flushed out of the reactor more easily. The V/III ratio is a measure of the ratio between how much group V-related precursor material is introduced into the reactor compared to how much group III-related precursor material. The V/III ratio is obtained by dividing the sum of all molar fractions from the group V sources by the sum of all molar fractions from the group III sources (eq. 2.7).

$$V/_{III} = \frac{\sum_1^n \chi_{i,group\ V}}{\sum_1^m \chi_{i,group\ III}} \tag{2.7}$$

where n, m are the number of sources of each group being used.

For the growth of ternary materials it is sometimes necessary to consider the ratio between molar fractions of the individual, isovalent species in the vapor phase and compare it to the ratio between the corresponding species in the crystalline phase, read “nanowire”. In this project we differentiate e.g. between the ratio of PH_3 and TMSb in the vapor phase and the corresponding ratio of P and Sb in the nanowire. The ratio for this project is defined as eq. 2.8;

$$\frac{\chi_P}{\chi_P + \chi_{Sb}} : \frac{\chi_{Sb}}{\chi_P + \chi_{Sb}} \tag{2.8}$$

Chapter 3

Electron microscopy

The dimensions of nanowires e.g. the diameter and crystalline phase changes along the growth direction of the nanowires are typically beyond the resolution limit of the best optical microscopes and thus require more powerful methods to be analyzed and imaged. Analysis techniques like scanning electron microscopy (SEM) and transmission electron microscopy (TEM) are used to investigate nanowires. It is important to know how these microscopy techniques work to interpret the information they provide. To observe an object in a light microscope it is important that light interact in some way with the object or it will remain invisible. In electron microscopes electrons serve as "light" and electrons have a special property. Electrons have the ability to behave both as charged particles and as waves with a particular amplitude and phase [21 and refs within].

All electron microscopes are closed systems operated at high to ultra-high vacuum. They are all fitted with an electron gun; there are two types of guns; thermionic and field emission gun (FEG). In thermionic electron guns a filament (commonly tungsten (W) or lanthanum hexaboride (LaB_6)) is heated and electrons are emitted through thermionic emission. Field emission guns have a sharp tip-shaped single crystal made from tungsten. A high voltage is applied to the tungsten tip making it acts as a cathode and emit electrons via field emission. The electrons are continuously emitted and accelerated towards the sample in the form of a beam. FEG has several advantages over thermionic sources; it has a longer lifetime and generates a more intense beam with a more well-defined wavelength [21 and refs within].

The beam is focused and controlled by a series of electromagnetic lenses and as the electrons reach the sample several forms of interaction can occur between the sample and the electrons. When considering the electron as a charged particle it has a velocity, direction and energy, the electron can then interact with both the atom core and the electron cloud surrounding it by Coulomb interaction(s) or by collision(s). An image of the interactions an electron can have with a substrate is shown in figure 3.1. If the electron maintains its energy and velocity but changes direction it has undergone an elastic scattering event. How much it changes direction is highly proportional to the atomic number of the material, the higher the atomic number, the more positively charged core and the stronger the Coulomb force. An elastically scattered electron can scatter 0-180°. If the electron is scattered <90° it is referred to as forward scattering and >90° backscattering and these are used in different ways to form images [21 and refs within].

An inelastic scattering event is then naturally when the electron changes both its direction and velocity and has transferred some of its energy to the sample. There are several ways that energy can be transferred to the sample and are in different ways useful to understand the sample. Among the most important ones in electron microscopy is the generation of secondary electrons, ionization of atoms and the emission of white radiation, bremsstrahlung. Secondary electrons are generated when the electron beam excites a valence electron from the sample to a free state. Secondary electrons have very low energy, in the order of a few eVs and only those generated close to the surface (few nm) will be able to leave the sample and be used for imaging and analysis. When an atom is ionized by exciting a core-shell

electron the atom will attempt to relax and return to its ground state, this is done by filling the core-shell state with an electron from a lower binding energy state shell, by doing so the atom may emit an X-ray with energy equal to the difference between the two energy levels involved in the relaxation. These X-rays will be unique to the element and are therefore known as characteristic X-rays. White radiation or bremsstrahlung is radiation generated by electrons in the beam being decelerated by atomic nuclei. Inelastic scattering will eventually lead to sample damage and is used for both imaging and chemical analysis of samples [21 and refs within].

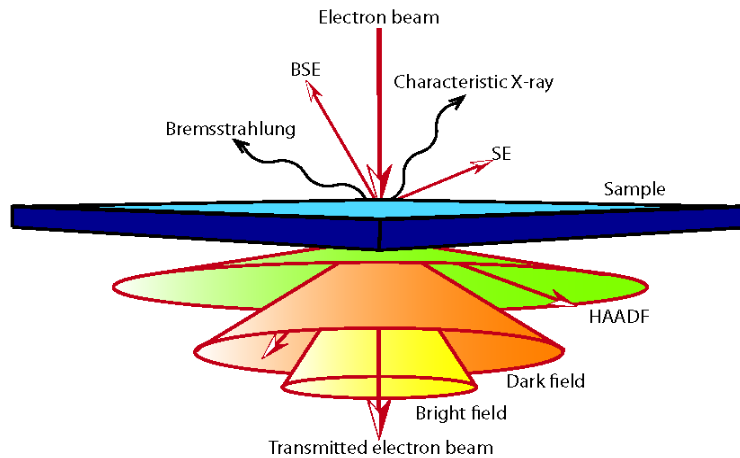

Figure 3.1 Overview of beam-sample interactions in electron microscopy.

Electrons can also be considered as waves and when a wave interacts with an object it is thought of as being diffracted much like light would be. Diffraction is a very strong tool in determining samples crystallographic characteristics e.g. crystal structure, lattice parameters and symmetry. Diffraction patterns can be used to orientate the sample incase a certain direction is desired for analysis or when a direction is to be analyzed. Figure 3.2 show a Fast-Fourier transform (FFT) of a ZB nanowire that has been tilted into the [011] beam direction to observe the stacking planes (ABCABC) in the nanowire.

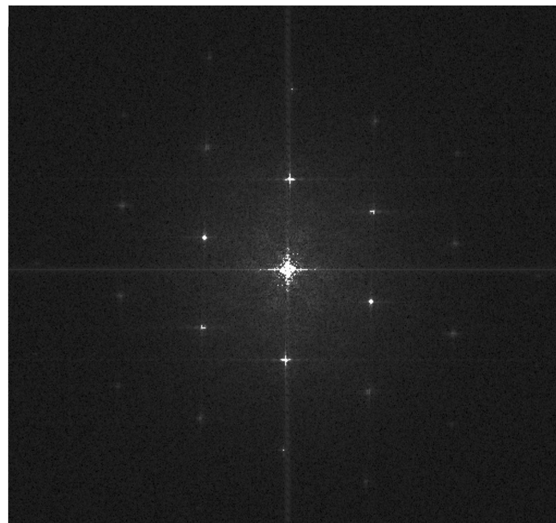

Figure 3.2 Fast-Fourier transform (FFT) pattern of a ZB nanowire with a [011] beam direction.

3.1 Scanning Electron Microscopy (SEM)

In scanning electron microscopy the samples are investigated by means of a scanning electron beam. SEM typically uses “thick” samples and it is a surface sensitive method. During this project SEM was the first tool used to determine the result of a growth experiment and provided valuable information about the grown sample e.g. the state of the nanowires grown. A SEM can give information about lengths, diameter and orientation of surface facets through contrast differences. The SEM can use secondary electrons and/or backscatter electrons to form images. Since secondary electrons are generated close to surfaces they are used in SEM to form topographic images as a function of beam position, the image is a recreation on account of a secondary electron detector counting the amount of electrons not their origin. The SEM used during this project have two SE detectors, one in the column and one on a side wall, referred to as the InLens detector and SE detector respectively. An example of the images that can be obtained with the InLens detector is shown in figure 3.3. The scattering probability of electrons increases with increasing sample thickness and for higher atomic number elements at constant sample thickness. The backscatter signals arising from this combination can be used to get images with a rough contrast difference depending on the chemical composition of the sample. The two imaging methods can be combined to get a topographical and compositional resolution.

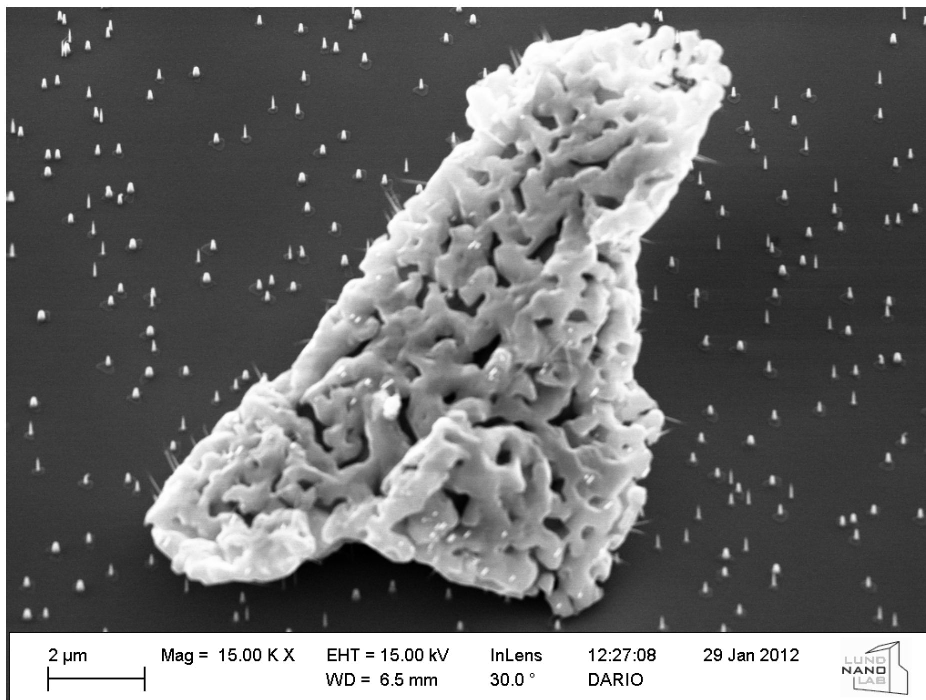

Figure 3.3 Sample contamination imaged at 30° tilt with the InLens detector after growth of nanowires. The contamination occurred before the Au particles were deposited which can be observed by the presence of grown nanowires on the surfaces of the contamination.

3.2 Transmission Electron Microscopy (TEM)

Sometimes investigation of individual segments of a sample e.g. crystallographic phase transitions on an atomic scale are needed or wanted and a more powerful microscopy technique is required. Transmission electron microscopy or TEM uses a highly accelerated electron beam (commonly 80kV-300kV) to probe samples and achieve a higher resolution than possible in any other electron microscopy technique. The purpose of the first set of electromagnetic lenses in a conventional TEM is to create parallel beam conditions. The parallel beam hits the sample and interacts according to the mechanisms discussed in section 3 above. Imaging is performed by detecting the interference between the unscattered beam and the scattered beams. After having passed the sample, the transmitted beams pass another set of electromagnetic lenses that project and magnify the image. The image can be observed in real time by allowing the electrons to hit a fluorescent screen or it can be viewed and recorded by having the transmitted beams hitting a CCD camera. What is observed is a two dimensional shadow projection of the three dimensional sample averaged over the entire thickness [21 and refs within]. Shadow projection refers to the fact that the unscattered beam is bright and at any point where the beam has been scattered appear with lower intensity in the image. Considering that scattering centers appear dark and that in a thick sample the electrons can scatter more than in a thin sample of identical material than that leads to the conclusion that a TEM requires thin samples, making nanowires perfect candidates due to being on the order of a few tens of nanometers in diameter.

High-resolution TEM or HRTEM is a mode in TEM. The mode is possible because of the electrons wave nature. Images in HRTEM are constructed solely from the interference between diffracted beams and

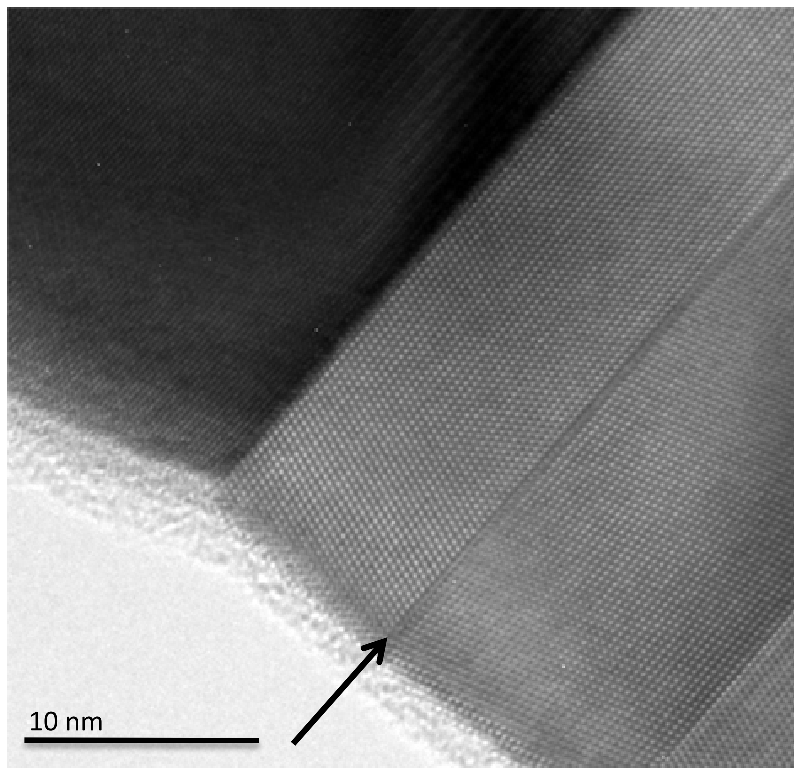

Figure 3.4 HRTEM image showing a section of a Au-Ga alloy particle (dark area) and a twin plane stacking defect (highlighted by the black arrow) in a ZB crystal structure.

not by any absorption that may have happened when electrons penetrated the sample. Figure 3.4 is an example of a HRTEM image that has [011] viewing direction and where the stacking sequence of ZB (ABCABC) can be observed.

By condensing the beam into a focused spot another mode is possible, so-called scanning TEM or STEM. The spot is referred to as a probe and can be between a few nm to less than a nm in size. The probe is then scanned across the sample much like a SEM, however it still uses transmitted electrons to create images. Typically the forward scattered electrons are considered as three categories for imaging in STEM, bright field (BF), dark field (DF) and high-angle annular dark field (HAADF). Bright field is much like the conventional TEM and uses the unscattered beam and the electrons typically scattered by up to 10 mrad. Imaging by HAADF and dark field do not use the unscattered beam and typically HAADF uses electrons scattered between 50 and 200 mrad and dark field ~10-50 mrad. Scattering is proportional to the square of the atomic number which means that in dark field imaging materials with higher average atomic number are imaged with higher contrast than materials with lower average atomic number at similar sample thickness and density. HAADF imaging uses only the highly scattered electrons to create images. All three imaging techniques create micrographs in the same way, imaging the sample by counting the detected electrons as a function of the probes position, much like a SEM [21 and refs within].

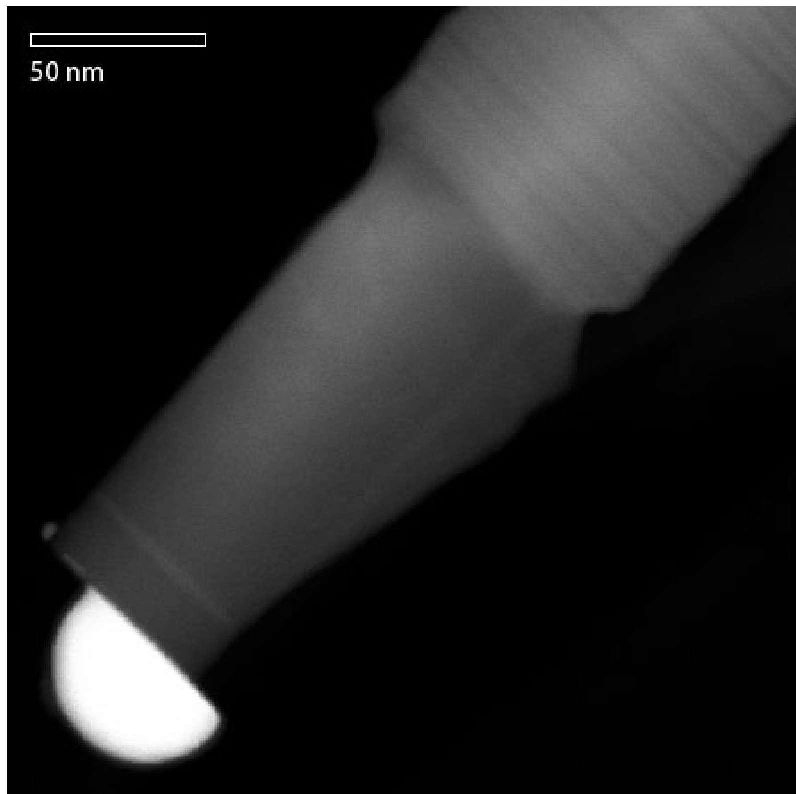

Figure 3.5 STEM-HAADF image of a GaP/ Ga($P_{1-x}Sb_x$) heterostructure showing overgrowth and stacking faults (lower contrast lines) in the GaP base (upper right corner) and an almost homogeneous intensity top Ga($P_{1-x}Sb_x$) where the Au-Ga-alloy particle (high contrast) is displaced from the centered position at the top of the nanowire.

3.3 Analytical Electron Microscopy and X-ray Energy-Dispersive Spectroscopy (EDS)

When the electron beam hits the sample and is inelastically scattered, energy is transferred to the sample and characteristic X-rays are emitted from the sample. They allow for precise determination of a samples chemical composition, quantitatively and qualitatively. The method is called X-ray energy-dispersive spectroscopy (EDS) and it can be combined with both SEM and TEM by introducing a special detector to the microscopes [22]. It is not only characteristic X-rays that are emitted from the sample but also bremsstrahlung when electrons are being decelerated by the sample. For quantitative analysis it is required to do a subtraction of the bremsstrahlung or the results will not be accurate. The final quantitative analysis yields the weight or atomic percentages of elements present in the sample. The detectors working principle is based on the creating of an amount of electron-hole pairs proportional to the energy of the incoming X-ray. Two X-rays can reach the detector at once resulting in twice as many electron-hole pairs and an error in the results. The electron-hole pairs can give off enough energy to excite the silicon atom in the detector resulting in a silicon X-ray being emitted and thus a silicon signal when that X-ray gets detected. Inelastic scattering will eventually result in sample damage; evaporation of material can be the results if the observed area is exposed for too long. Typically 1-2% standard deviation is expected in the results from the EDS detectors [21 and refs within].

When combining EDS with a conventional TEM an average of the exposed areas composition is obtained. This arises from the fact that conventional TEM is a stationary parallel beam and exposes a rather large area. More detailed information can be obtained by combining with a STEM by reducing the beam to a sub nanometer probe and scanning across the sample. STEM allows for mapping of selected characteristic X-ray lines over line(s) and/or region(s) of the specimen by scan control. STEM can also be used to do point analysis by making the probe stationary. It is also possible to combine EDS with a SEM and it has the same possibilities as with the STEM at a cost of lower spatial resolution.

Chapter 4

Gallium phosphide antimonide

Gallium phosphide antimonide ($Ga(P_{1-x}Sb_x)$) can be considered as a mixture of gallium phosphide (GaP) and gallium antimonide (GaSb). These two materials span over a large region of possible lattice parameters, from 0.54505 nm (GaP) to 0.609593 nm (GaSb). The resulting bandgap can be both indirect (GaP) and direct (GaSb) with a predicted transition point around 35% Sb ($Ga(P_{0,65}Sb_{0,35})$) and with an energy ranging from 2.26 eV (GaP) to 0.726 eV (GaSb) [23,24].

Any growth study begins with attempts to obtain a starting point based on prior experience and understanding of similar material systems and then branch out from there. In the case of $Ga(P_{1-x}Sb_x)$, work on GaP, GaSb and other Sb-containing binary and ternary material systems were used as a foundation for the growth experiments [25-43]. Growth of GaSb-containing materials on a substrate is difficult due to Sb wetting properties [44 and refs within] and the solution is growth from a stem. Three Ga-based binaries are lattice matched across the composition range of $Ga(P_{1-x}Sb_x)$ namely GaP, GaAs and GaSb. GaAs substrate was excluded to avoid arsenic contamination. GaSb substrate would decompose during the annealing step of the growth due to the low melting point and originate in the growth difficulties from the resulting Sb surface wetting. Thus GaP substrate and stem was used for the growth experiments.

4.1 Lattice mismatch

The lattice mismatch is the difference in lattice parameter of two materials. GaP and GaSb is the most lattice mismatched combinations among the III-V materials. The resulting lattice mismatch between GaP and GaSb is 11.8%.

$$Lattice\ mismatch = \frac{Lattice\ parameter\ of\ the\ top\ material}{Lattice\ parameter\ of\ the\ base\ material} - 1 \qquad (4.1)$$

For any composition ($0<x<1$) of $Ga(P_{1-x}Sb_x)$ grown on a GaP stem the resulting lattice mismatch would be less than that of GaSb on GaP. Thus to establish if the lattice mismatch would be a limiting factor for growth of $Ga(P_{1-x}Sb_x)$ on a GaP stem a growth experiment where GaSb was grown on a GaP stem was conducted. The growth experiment showed a yield of ~10% of straight GaP/GaSb nanowires and that it is possible to grow $Ga(P_{1-x}Sb_x)$ with any composition on GaP but reveal very little information about the limitations and difficulties in the growth of $Ga(P_{1-x}Sb_x)$ on GaP. Apart from the straight nanowires figure 4.1 show a higher fraction of the nanowires (~40%) where it seems the Au particle wets the side facets of the GaP stem and have slid off the nanowire when Sb was introduced, resulting in growth along the surface.

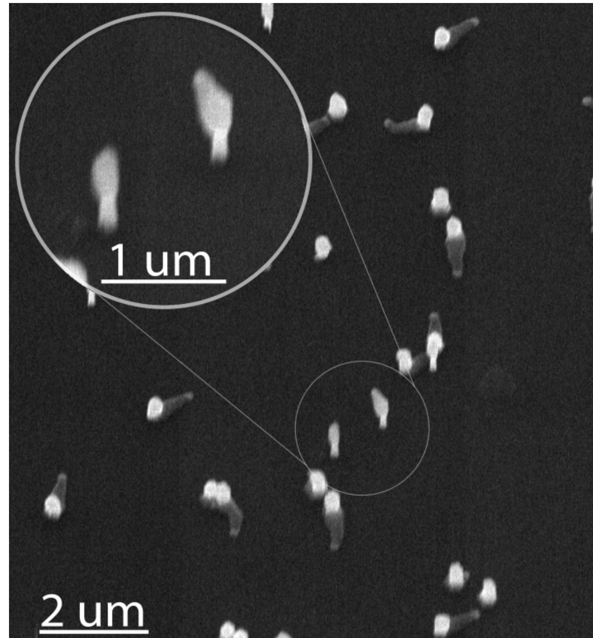

Figure 4.1 SEM image of a sample with 15 min of GaSb growth on 250 nm GaP stem with a 30° tilted view. A low yield (~10%) of straight wires can be noticed as well as a higher fraction (~40%) of particles which are off-positioned from the nanowire top and induced growth at the surface.

4.2 Surfactant effect

Sb has a higher atomic number and a larger atomic radius compared to other materials commonly used in III-V growth. Howard et al put it bluntly "Sb is rejected from incorporation into the solid due to their large size and can be used to change the physical and chemical processes occurring at the growing surface." [31] In this work and others they have shown how Sb can affect growth and incorporation of materials by being present in small concentrations. Sb has a low vapor pressure [45] which results in much lower desorption than adsorption on the surface of the substrate or nanowire which may affect other materials ability to diffuse on the surface [26, 31]. This behavior is called a surfactant effect and is a major issue with epitaxial growth of Sb-based materials.

To be sure of reproducible results, a reliable removal of Sb is required in between each growth run as any Sb contamination in the growth reactor will affect the adjacent growths runs. A high temperature etching step using HCl as an etching agent followed by deposition of a GaP protective layer was carried out before each actual growth run in order to maintain reliable and reproducible process conditions. The growth experiments performed show a decrease of the growth rate from 60 nm/min (stem) to 10 nm/min (ternary segment) after introducing TMSb to the reactor. The growth rate is based on the growth time and the lengths determined by SEM investigation and assume an instant nucleation, meaning that during the entire growth time the nanowire was growing. The growth rate decreased from 10 nm/min to 2 nm/min as the nominal input flow of TMSb was increased from 0.013 mmol/min to 0.078 mmol/min. Values are calculated from Appendix A and figure 4.8 b).

4.3 Growth series, effects and limitations

Several growth series were performed and during each series the gas flow of one source was changed in regular intervals while all other parameters were kept constant. A common starting point for the series was developed and each growth series started with the parameter setting of the starting point and then one source was stepped. This was done in an attempt to get information on the effect of the different sources on the growth rate. A flow chart of the relative molar fractions of the different series can be found at the end of Appendix A. To analyze the composition in the nanowires EDS was performed in a TEM. Tables with measured composition obtained from EDS spectra for each series can be found in Appendix B.

4.3.1 Gallium growth series

For the TMGa series the molar flow of TMGa was increased from 4.68 µmol/min to 18.71 µmol/min in increments of 4.68 µmol/min. The results suggest that the growth rate is at least partially limited by the group III precursor flow. A square fit to the length increase fit best with the measured lengths suggesting a larger length increase as TMGa is increased. It has been shown in previous work [18, 19] that temperature influences the rate of axial and radial growth for various reasons e g adatom trapping. Therefore the growth rate does not have to be linearly dependent on the molar fraction at a given temperature as there is a limit on how fast adatoms can be trapped. In figure 4.2 the length of the nanowires determined by SEM investigations is plotted against the nominal input molar fraction of TMGa. A linear and a square fit has been inserted with the data points and the square fit correspond better to the data points and is supported by the results of the previous work.

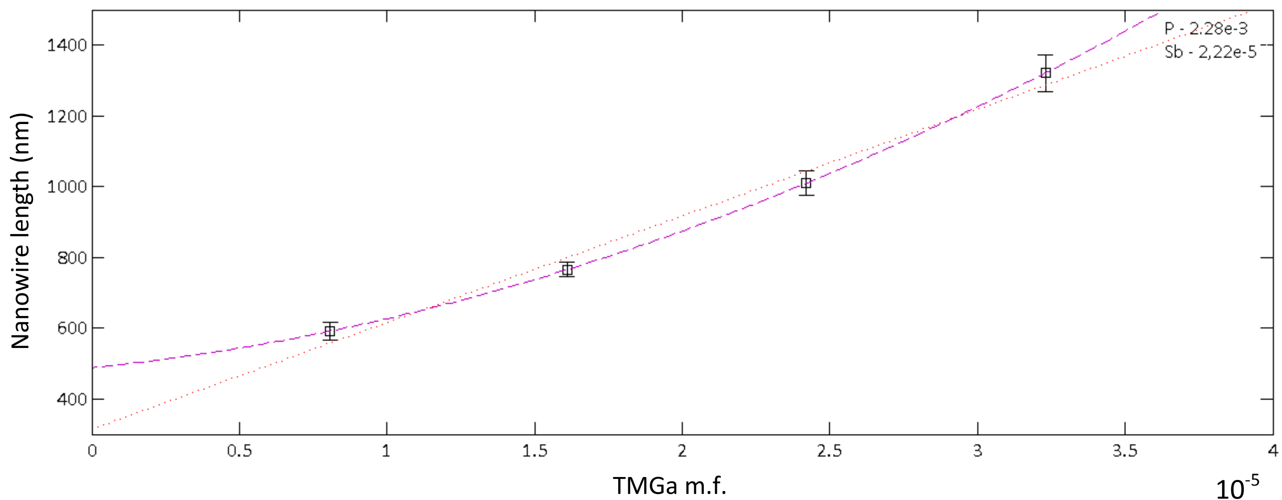

Figure 4.2 Average nanowire length with standard deviation determined by SEM investigations for the TMGa series where the V/III ratio changes from 285 to ~71 going from left to right. Dotted line represent a linear equation fit to the data points and the dashed line corresponds to the square fit of length dependence against PH_3 m.f.

The EDS results from the starting point shows a Sb content in the nanowires of around 2±2% ($Ga(P_{0,98\pm0,02}Sb_{0,02\pm0,02})$)[1]. EDS was also performed on the end point of the TMGa series and the spectra show a Sb signal resembling the one from the starting point. The Sb content in the nanowires were found to be between 2±1% Sb ($Ga(P_{0,98\pm0,01}Sb_{0,02\pm0,01})$) however considering the region of the standard deviation of the detector it is hard to determine if the quantification difference between the starting point and the end point is statistically significant.

4.3.2 Phosphor growth series

For the PH_3 series, the molar fraction of PH_3 was reduced by a factor of two (2) from one step to the next where the difference between the first step and the last step is a factor eight (8) (see table B.3). The lengths of the nanowires in the series did not vary within the measurement accuracy in the interval of the PH_3 molar fraction where the series was performed, suggesting that the growth is not limited by PH_3 supply. For this growth series the relation between the PH_3:TMSb (eq. 2.8) in the vapor phase range from around 100:1 to 10:1, right to left in figure 4.3. The lowest PH_3 flow used is at the mechanical limit of the MFC used (5 sccm on a 200 sccm MFC) and hence it was not possible within this study to determine the region in which PH_3 starts to affect the growth rate.

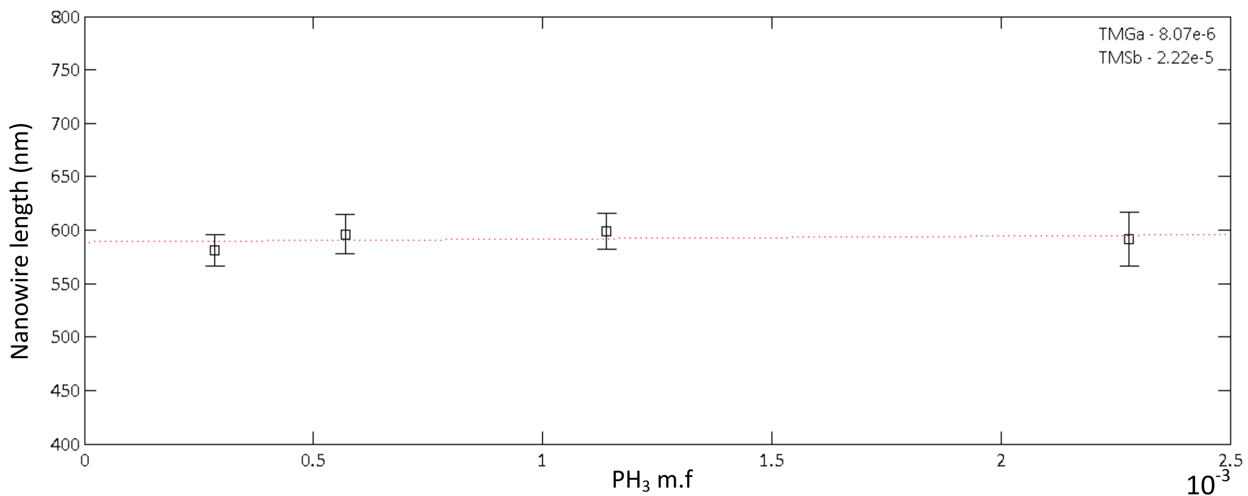

Figure 4.3 Average nanowire length with standard deviation determined by SEM investigations for PH_3 series. The V/III ratio in the image varies from 38 (left side data point) to 285 (right side data point). Dotted line is a linear equation fit showing a small or absent dependence of the nanowire length against PH_3 m.f.

While no indications were found for a correlation between the molar fraction of PH_3 and the length of the nanowires, it was however not clear whether variations in the molar fraction of PH_3 affect the incorporation of Sb into the nanowires. The EDS results of the growth series show a slight tendency towards an increase in Sb incorporation in the nanowires for lower PH_3 molar fractions. While in the low PH_3 molar fraction side of the growth series the EDS results show a 5±2% Sb incorporation ($Ga(P_{0,95\pm0,02}Sb_{0,05\pm0,02})$) in the nanowires, a small but significant increase in Sb compared to the starting point (2±2%). The conclusion is then that there is a tendency towards that lowering the PH_3 molar

[1] Composition is calculated as $Composition\ Sb = \frac{EDS(Sb)_{at\%}}{EDS(Sb)_{at\%}+EDS(P)_{at\%}}$

fraction allows for more Sb incorporation into the nanowire without reducing the overall growth rate in the PH_3 interval.

4.3.3 Antimony growth series

The TMSb series was done by evenly stepping the TMSb molar fraction in between the value of the starting point and the highest molar fraction possible without changing the pressure in the bubbler (see table B.5). The lengths of the nanowires vary between the two end points and that of the points in between. With the available data it is not conclusively possible to determine the cause for the variation in overall nanowire lengths as no change in the morphology of the nanowires was detected e.g. nanowire width and crystalline phase.

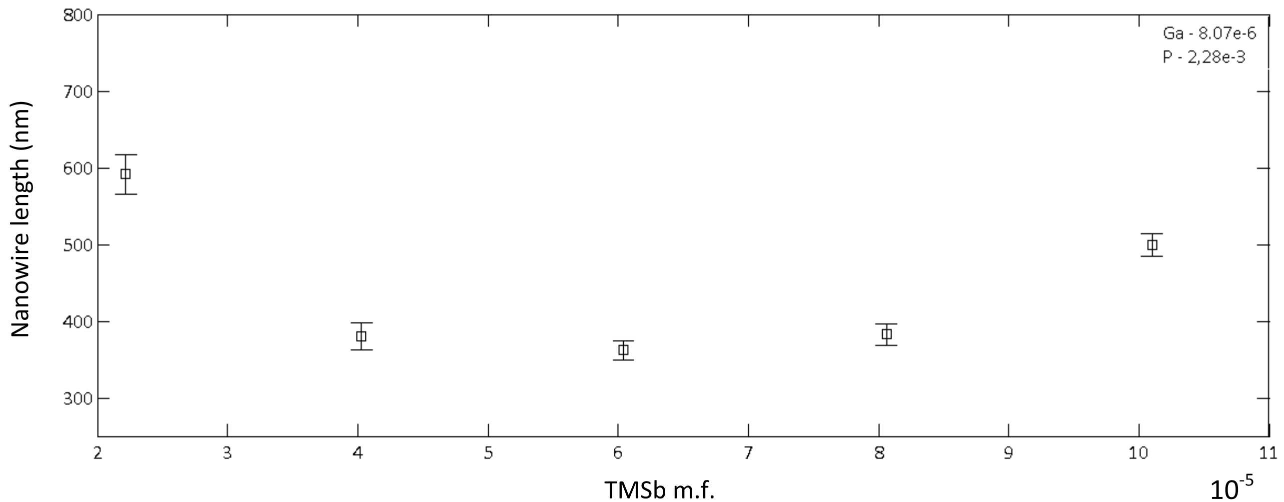

Figure 4.4 Average nanowire length with standard deviation determined by SEM investigations for TMSb series where the V/III ratio changes from 285 to 295 going from the left data point to the right data point.

From the EDS analysis we concluded that the measured Sb (2±1%, ($Ga(P_{0,98\pm0,01}Sb_{0,02\pm0,01})$)) content in the nanowires is about the same as for both the starting point (#4676 in table B.2) and the TMGa end point (#4838 in table B.3). This value is remarkable since the relation (eq. 2.8) between PH_3:TMSb in the vapor phase ranges from 100:1 to 20:1 (from left to right in figure 4.4). The ratios are similar to the PH_3 series while the composition is different.

4.4 Growth challenges

The different growth series provided the information that the applied changes in PH_3 molar fractions did not show a measurable effect on the growth rate in the chosen interval. A different behavior was observed for the TMGa with higher growth rate for increasing TMGa molar fraction although a non-linear trend was found. The TMSb series results were puzzling and with getting no further than 7% Sb incorporation in the nanowire the pressure in the TMSb bubbler was lowered in order to increase the molar fraction of Sb in the vapor phase. This was the best option as with the minimum stable PH_3 molar fraction a 1:1 ratio (eq. 2.8) between the two materials molar fraction was possible. Combining this plan with the increased growth rate from raising the TMGa molar fraction two miniseries were carried out,

one with the original low TMGa molar fraction and one with high TMGa molar fraction. Both miniseries used the same variations in TMSb molar fraction and the relation between PH_3 and TMSb in the vapor phase for the two miniseries was 1:1 and 7:3, respectively.

For the low TMGa molar fraction experiments no clear ternary segment is visible on the nanowires by SEM. The nanowires are very short in both samples and it seems that low TMGa and high TMSb molar

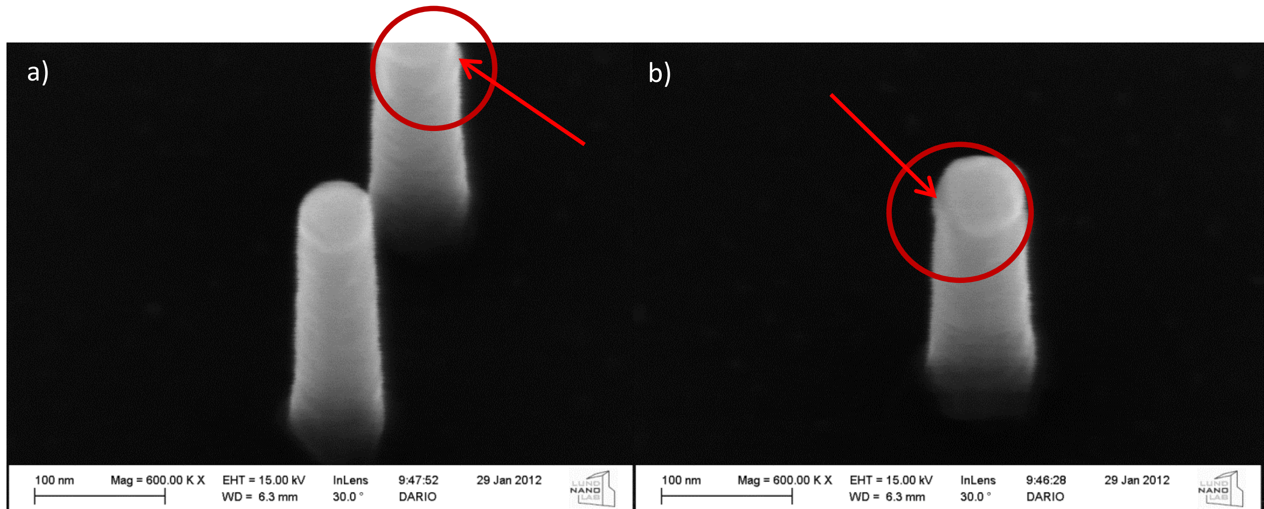

Figure 4.5 SEM images with a 30° tilt view of growth #5022 (table B.6) highlighting a small area on top of the nanowire where the Au-Ga-alloy particle (circular feature on top of the nanowires) seem to not fully wet the nanowire top facet with red arrows. Contrast differences in the nanowires are likely due to the mixed crystal structure of the GaP stem.

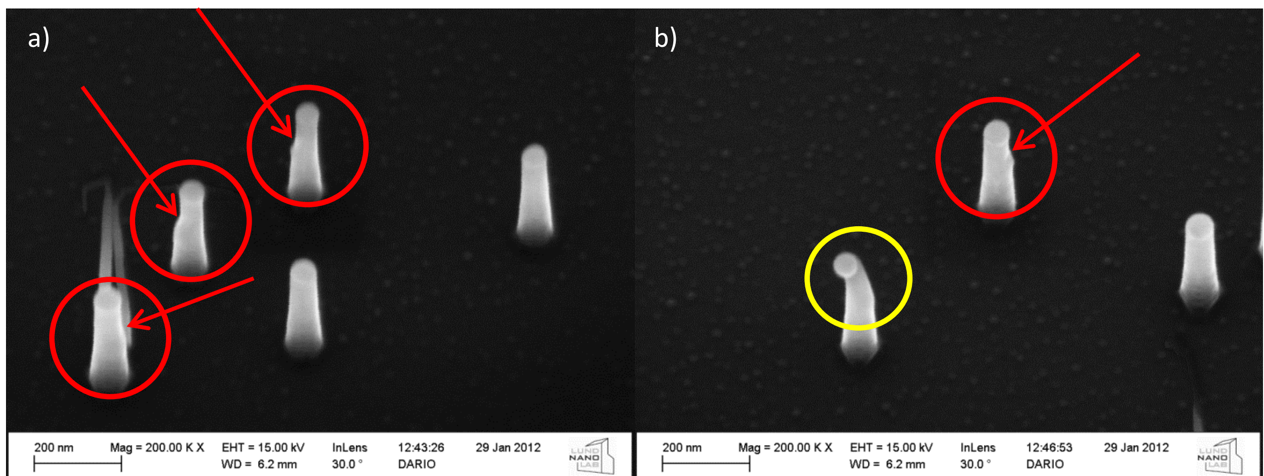

Figure 4.6 SEM images with a 30° tilt view of growth #5023. Red arrows and circles highlight the narrowing of the nanowires and the yellow circle highlight a kinked nanowire. Long thin self-seeded nanowires appear around gold-seeded nanowires with an increased probability with increasing gold particle size.

fraction results in a very low growth rate. The most interesting part of these nanowires is the area around the Au particle, shown in figure 4.5. A small area on top of the nanowire facet seems non-covered as if the Au-Ga-alloy particle not fully wetting the nanowire top facet. For the high TMGa molar fraction experiments a minor fraction of the grown nanowires were kinked, a known side effect when too much Ga is occupying the Au particle, shown in figure 4.6 b). All of the nanowires exhibit a narrowing

of the top part in the shape of a step when imaged with SEM. The step is highlighted by red arrows in figure 4.6 a) and b).

Figure 4.7 shows a nanowire investigated by TEM where inclined stacking defects were found and are formed along <111>-type directions. Dubrovskii et al [46] proposed a model for nanowire nucleation which can explain the formation of the inclined stacking defect as an event that occurs when there is a significant chance of polynucleation occurring in a single layer as a result of a low growth rate. One such misfit would propagate the entire nanowire. The appearance of this stacking defect has been imaged by TEM in all nanowire growth experiments with a ratio between PH_3 and TMSb lower than 30:1 indicating a relation between TMSb molar fraction and the probability non-aligned polynucleation in a single layer. However at this point it is not clear how the polynucleation is related to the TMSb molar fraction.

Figure 4.8 a) contain a plot of the length of the nanowires determined from SEM investigation versus the molar fraction of TMSb for the TMSb series and the miniseries. The graphical evaluation of figure 4.8 a) suggest an inconsistency in the length with respect to the TMSb molar fractions. This highlights the need to accurately measure the ternary length segments by TEM. The ternary length segments measured by TEM are plotted in the figure 4.8 b) and suggests a tendency towards a linear dependence on the molar fraction of TMSb with the data available. Having a higher TMGa molar fraction seem to increase the length of the ternary segments but has a rapid decrease the higher the corresponding TMSb molar fraction gets. The growth experiments with a higher PH_3 molar fraction indicate a faster reduction in ternary growth rate as a function of TMSb molar fraction than that of the low PH_3 molar fraction growth experiments. With the few data points available it is not possible to give a conclusive dependency but all three series exhibit similar results.

EDS measurements were performed on the miniseries and the nanowires in all samples showed a 6±1% Sb incorporation ($Ga(P_{0,94\pm0,01}Sb_{0,06\pm0,01})$) in the ternary segment, similar to the previous growth series leading to the conclusion that there is a maximum amount (~7%) that can be incorporated into the

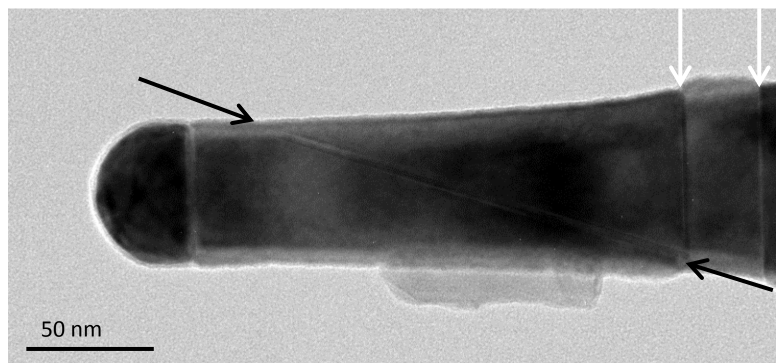

Figure 4.7 Nanowire from growth #5024 imaged by TEM at 86100 magnification. Dark hemisphere on the left side of the image is the Au-Ga alloy particle and on the right side of the image a series of twin plane stacking faults can be seen, highlighted by white arrows. Black arrows highlight the inclined stacking defect found in growths with a PH_3:TMSb ratio >7:3.

ternary structure by growing from a GaP stem even when using such a high molar fraction of TMSb for the applied experimental conditions. Borg et al [42] reported a correlation between the variation in vapor phase composition of TMSb and AsH_3 and the incorporation of Sb in InAsSb nanowires for various V/III ratios and found that for increasing nominal V/III ratio the incorporation becomes strongly dependent on vapor phase composition and it is very likely that within the presented study a necessary ratio between the molar fractions of PH_3 and TMSb was not reached which would have led to a similar correlation as reported.

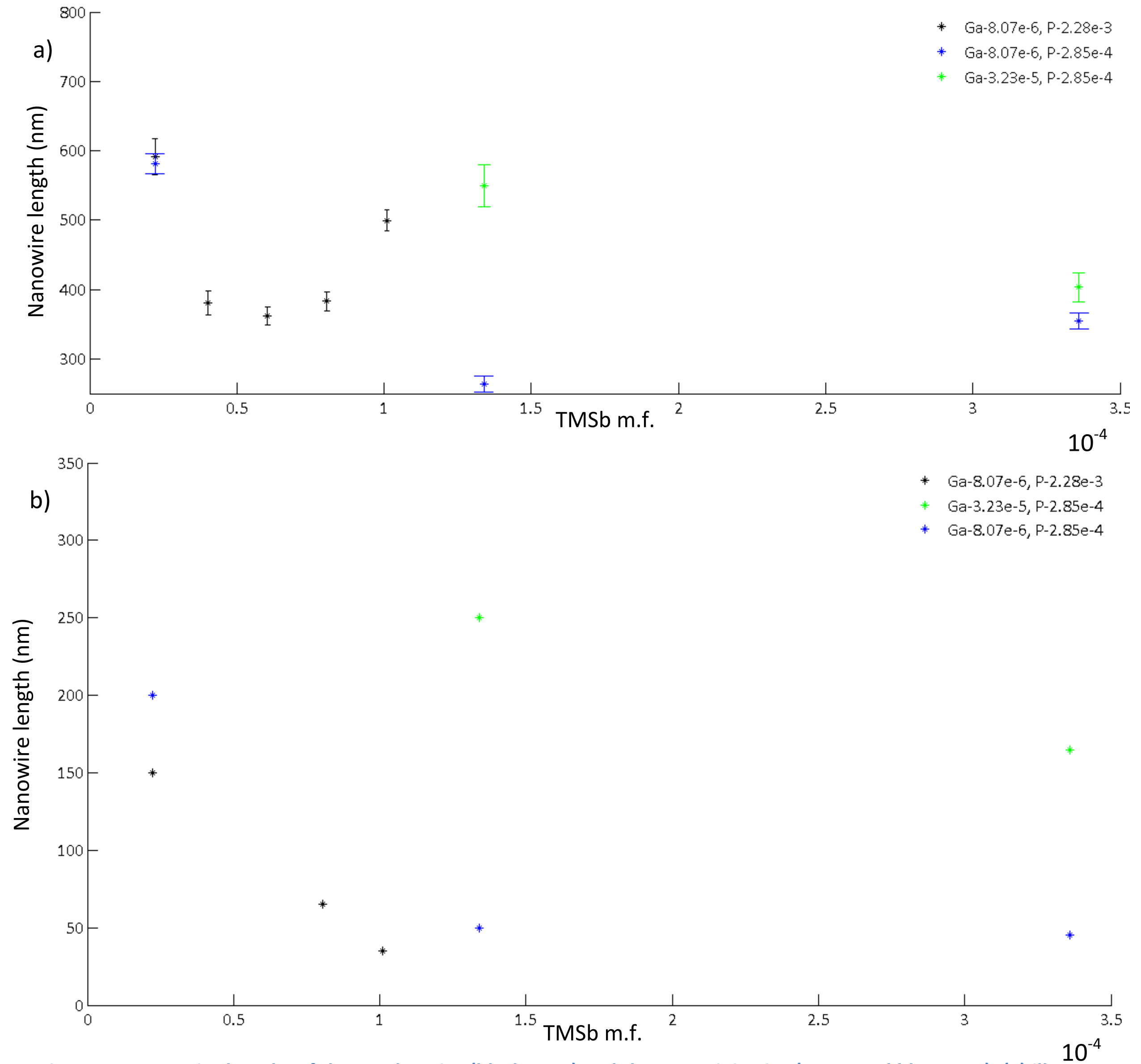

Figure 4.8 Nanowire lengths of the TMSb series (black stars) and the two miniseries (green and blue stars). (a) illustrates the total nanowire length determined by SEM investigation and (b) show the ternary length measured by TEM investigations. The fixed TMGa and PH_3 m.f. are shown in the upper right corner of each graph and the V/III ratio varies in both graphs for the black stars from 285 to 295, for the blue stars from 38 to 77 and for the green stars from 13 to 19.

4.5 Seed particle and Crystal structure

One of the properties Sb as a material is known for is the ability to promote ZB crystal structures in nanowire growth even at relatively low concentrations. Xu et al [35] have shown that Sb in InAs turns the structure from pure WZ to pure ZB by adding 12 at% Sb ($In(As_{0,88}Sb_{0,12})$) and that the structure transition starts at a level of Sb which is below the EDS detection limit. With the parameter settings used during this project it is easy to observe the effects by comparing the structural properties of the stem (GaP) and the ternary segment ($Ga(P_{1-x}Sb_x)$) as seen in figure 4.9. The stem has a mixed ZB-WZ crystal structure while the crystal structure property of the ternary segments is identical for all nanowires investigated, a ZB crystal structure characterized by a low density of stacking defects or an absence of stacking defects in the range x=4±3 % Sb.

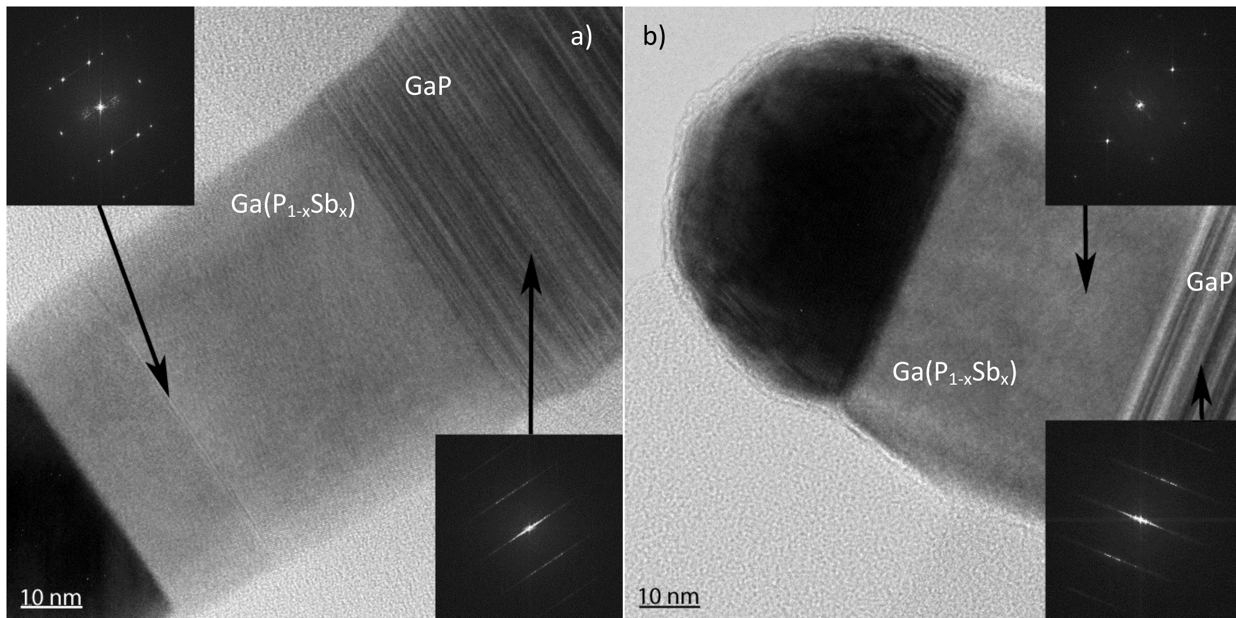

Figure 4.9 Nanowires imaged by TEM, showing the Au-Ga alloy particle (dark area). Both nanowires exhibit a mixed ZB-WZ crystal structure in the stem illustrated by the inserted FFT diffraction pattern (lower right corners). Ternary segment in (a) show a diffraction pattern from the twinplane stacking defect (highlighted by a black arrow) in a ZB crystal structure nanowire with a 2±1% Sb composition in the ternary segment. The ternary segment in (b) show ZB crystal structure free of stacking defects with diffraction pattern with a 6±1% Sb composition in the ternary segment. The viewing direction in both images and all diffraction patterns is$\langle 1\ 1\ 0 \rangle$.

A large variation in the Au-alloy particle composition after growths was measured. The Ga as group III is present in the particles from ~0 to 25%. The Ga content in the Au particle during growth, should be close to the measured value since the growth it terminated by turning of all sources and cooling under H_2. This leaves no room for depletion of the Au particle, unlike cooling under group V overpressure where typically a short segment grows known as the neck region. In contamination has been found in all Au particles while no In was detected in the nanowires, this is likely from a small In contamination in the reactor, which source is unknown at this time. It has been suggested by Johansson et al [47] that a slight In contamination can affect the growth rate for GaP as well as the structure and that it can likely be contributed to the inability of Ga to replace In in the Au-alloy and thus Ga cannot occupy the Au particle in the same manner as it can in the absence of In. In the case of $Ga(P_{1-x}Sb_x)$ the contamination of In in the

Au particle disrupts Sbs ability to promote ZB crystal structure absent of stacking defects in the $Ga(P_{1-x}Sb_x)$ segment of the nanowires. The formed stacking defects resulting from the In contamination can be seen in figure 4.10. However it is not possible to conclusively determine if the In contamination affects the growth rate of $Ga(P_{1-x}Sb_x)$. The presence of In does not seem to influence Sb or P solubility in the Au-alloy as we have observed similar Sb and P content for the samples with and without the In contamination.

In the case where the ratio between PH_3:TMSb molar fractions were lower than 7:3, the Au-alloy particles have decomposed into two parts with different compositions, one with the previously seen Au_xGa_{1-x} composition and one with Au_xSb_{1-x} composition. In a few cases the Au_xSb_{1-x} part has formed a portion inside Au_xGa_{1-x} particle (figure 4.11 b)) and in the other cases it has formed its own particle ($AuSb_2$) on the side facet of the Au_xGa_{1-x} particle (figure 4.11 a)).

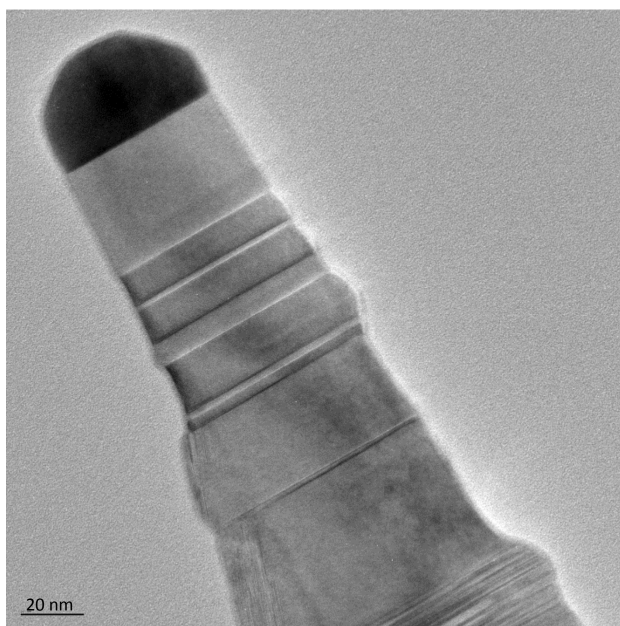

Figure 4.10 Nanowire imaged by TEM illustrating multiple stacking defects caused by In contamination in the Au particle (dark area). EDS show a composition of 32% In in the Au particle and a ~5 at% Sb content in the ternary segment. Lower right corner of the image show the mixed ZB-WZ crystal structure found in the stem.

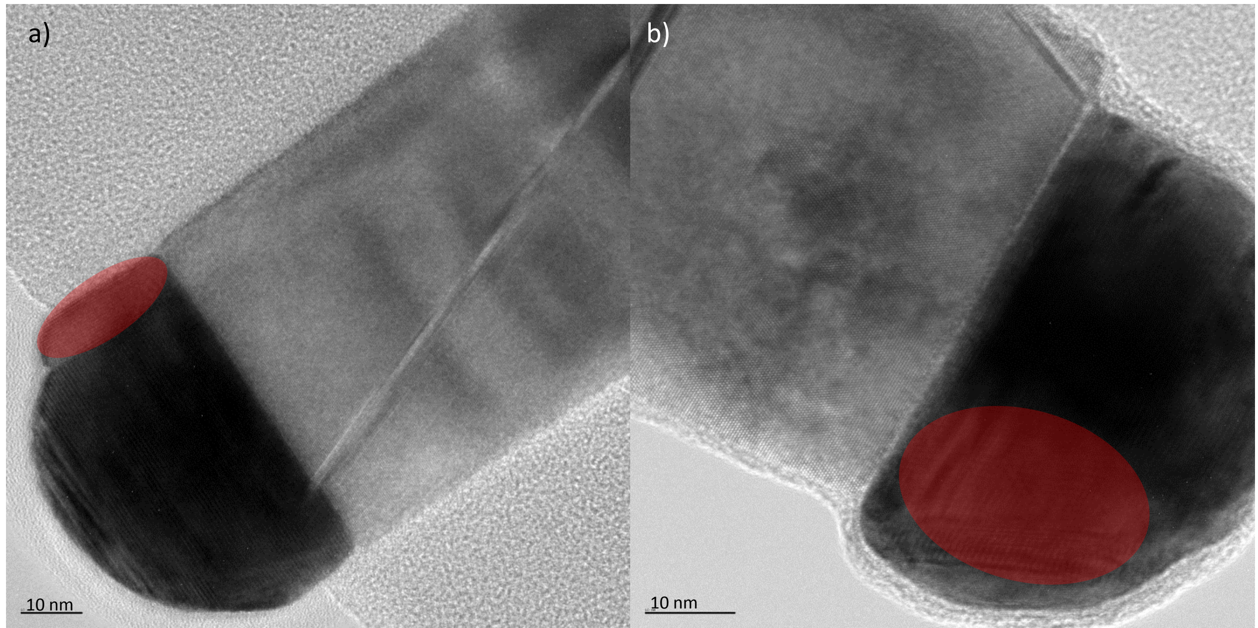

Figure 4.11 Nanowires imaged by TEM at (a) 285k and (b) 416k magnification. The dark areas are the Au-X-alloys and the red color indicates areas where a high Sb content was measured by EDS mapping. In (a) the Au-Sb-alloy have split off from the rest of the Au-Ga particle and in (b) the Au-Sb complex is mixed with the Au-Ga-alloy.

Chapter 5

Conclusions

We have presented the successful growth of $Ga(P_{1-x}Sb_x)$ on GaP stem with an incorporation of 7% Sb ($Ga(P_{0,93}Sb_{0,07})$). We have investigated GaP/$Ga(P_{1-x}Sb_x)$ nanowires grown by MOVPE and further investigated the grown nanowires by SEM, TEM and EDS techniques. The results presented indicate that the growth rate depends on the TMGa molar fraction (higher growth rate for increased TMGa molar fraction – but no linear dependency) and the TMSb molar fraction (lower growth rate for increasing TMSb molar fraction). Furthermore the stacking defect non-parallel to the growth direction have been imaged by TEM in all nanowire growth experiments with a TMSb molar fraction above 10^{-4} (ratio PH_3:TMSb of <30:1), indicating a relation between TMSb molar fraction and the probability of non-aligned polynucleation within a single layer.

The presence of Sb promotes ZB crystal structure formation in $Ga(P_{1-x}Sb_x)$ nanowires. The nanowires exhibit a low density of stacking defects at a measured Sb content of approximately 1% ($Ga(P_{0,99}Sb_{0,01})$) and defect free ZB crystal structure at ≤7% Sb ($Ga(P_{\geq 0,93}Sb_{\leq 0,07})$). We have observed that In contamination in the Au-alloy results in the disruption of Sbs ability to promote formation of ZB crystal structure absent of stacking defects in $Ga(P_{1-x}Sb_x)$ nanowires. In nanowires investigated by TEM where the ratio between PH_3:TMSb was lower than 7:3 the decomposition of the Au-alloy into two parts is observed in post growth investigations, one with the previously seen Au_xGa_{1-x} and one with Au_xSb_{1-x}. The EDS measurements indicate $AuSb_2$ composition of the Au_xSb_{1-x} part.

In conclusion we have presented the first steps in the effort of overcoming the 1-99% miscibility gap in the $Ga(P_{1-x}Sb_x)$ material system.

5.1 Outlook

$Ga(P_{1-x}Sb_x)$ nanowires are interesting and quite challenging material to grow. Further growth experiments are required to improve the understanding and control of Sb-based ternary materials. In this project we have shown how different molar fraction ranges affect the growth rate and incorporation. The properties and resulting impact on the crystal structure of Sb e.g. the surfactant effect, low vapor pressure, atomic radii etc. are challenges for growth of Sb-based binary and ternary material systems. With this project as a base there are several steps that need to be covered to get a better understanding of the $Ga(P_{1-x}Sb_x)$ material system;

- The project was based around growth of $Ga(P_{1-x}Sb_x)$ on a GaP stem. To provide stronger indications of whether or not the stem limits the incorporation of Sb into the nanowires. A plan would be to perform experimental growths with the same conditions on different stem materials such as GaAs or GaSb.
- The technical limitations of the machine setup used during this project imposed a limit on the ratio between PH_3 and TMSb and therefore the V/III accessible. Conducting growth experiments combining a reduction series of the PH_3 molar fraction to achieve a PH_3:TMSb ratio of 1:100

followed by a lowering the V/III ratio towards 1 by lowering the total group V flow, could result in the observation of a similar correlation between the vapor phase composition and the composition of the nanowires as have been presented for the InAsSb material system.

- We have shown that the growth rate of $Ga(P_{1-x}Sb_x)$ is limited by the molar fraction of TMGa and TMSb. Could the growth rate be limited by an extended nucleation time after switching to the ternary segment growth? A nucleation time test series could provide an answer, a series where the growths are terminated at different times after switching to the ternary segment growth.
- One of the most interesting results is the formation of two-phase Au-alloy particles with different compositions. To understand how, when and why this phase is formed will lead to a better understanding of the Au-Sb interaction during growth and is will support the understanding of how to control Sb incorporation and its interaction with other group III- and group V-related materials. It would be a valuable step in establishing whether this is a unique phenomenon growing $Ga(P_{1-x}Sb_x)$ on a GaP stem, or if another mechanism is responsible for the formation of two-phased Au-alloy particles.
- During the entire project the growth temperature was kept at 470°C. However, the temperature could significantly affect the $Ga(P_{1-x}Sb_x)$ nanowire growth behavior. We propose a growth series experiment to determine the effects of temperature on $Ga(P_{1-x}Sb_x)$ nanowire growth. This is a required step in establishing optimized growth conditions.

Appendix A

Growth parameters

In this section the parameters of each growth will be presented in full, accompanied by the growth number and SEM image of the growth. All growths were initiated with an annealing process under 50 sccm (standard cubic centimeter per minute) PH_3 at 630°C for 7 min, followed by a stem with 2 sccm TMGa and 40 sccm PH_3 for 2,5 min. Ternary structure grown for 20 min unless otherwise specified. All growths were terminated by closing all sources and cooling under H_2.

Growth temperature (°C)	470
Total reactor flow rate (*l*)	13
Reactor pressure during growth (mbar)	100

Table B.1 Parameters kept constant for all growths.

The source flows are written as "flow rate (sccm) / bubbler pressure (mbar)".

Starting point	TMGa	Molar fraction	PH_3	Molar fraction	TMSb	Molar fraction	V/III	PH_3:TMSb
#4676	2/1000	8,07e-6	40	2,28e-3	4,4/1000	2,22e-5	285	99:1

Table B.2 Growth parameters for starting point.

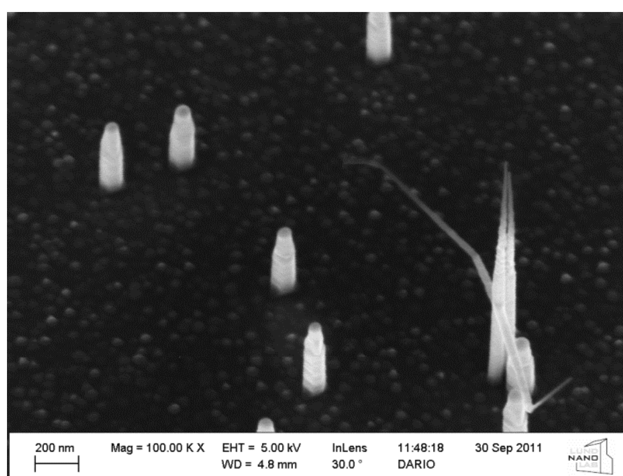

Figure B.1 100k magnification of starting point growth

PH_3 series	TMGa	Molar fraction	PH_3	Molar fraction	TMSb	Molar fraction	V/III	PH_3:TMSb
#4832	2/1000	8,07e-6	20	1,14e-3	4,4/1000	2,22e-5	143,9	49:1
#4833	2/1000	8,07e-6	10	5,69e-4	4,4/1000	2,22e-5	73,3	24:1
#4834	2/1000	8,07e-6	5	2,85e-4	4,4/1000	2,22e-5	38	12,9:1

Table B.3 Growth parameters for PH_3 series.

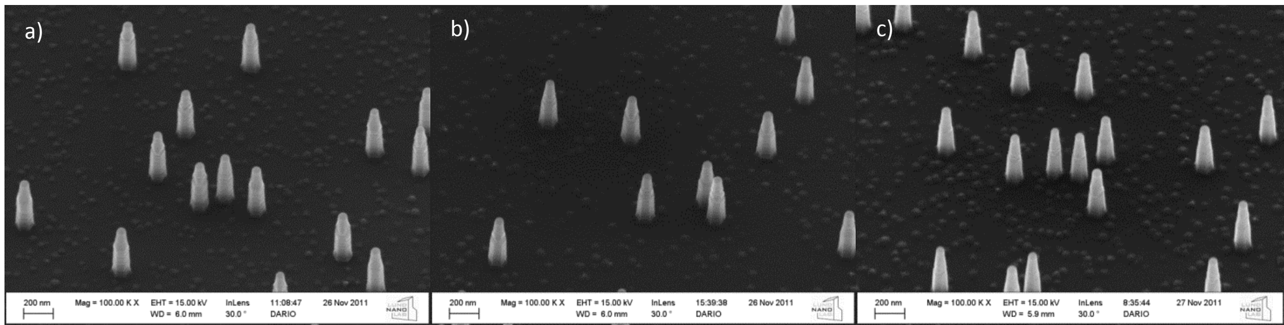

Figure B.2 Overview images of PH3 series at 100k magnification (a) #4832 (b) #4833 (c) #4834.

TMGa series	TMGa	Molar fraction	PH_3	Molar fraction	TMSb	Molar fraction	V/III	PH_3:TMSb
#4836	4/1000	1,61e-5	40	2,28e-3	4,4/1000	2,22e-5	142,5	99:1
#4837	6/1000	2,42e-5	40	2,28e-3	4,4/1000	2,22e-5	95	99:1
#4838	8/1000	3,23e-5	40	2,28e-3	4,4/1000	2,22e-5	71,3	99:1

Table B.4 Growth parameters for TMGa series.

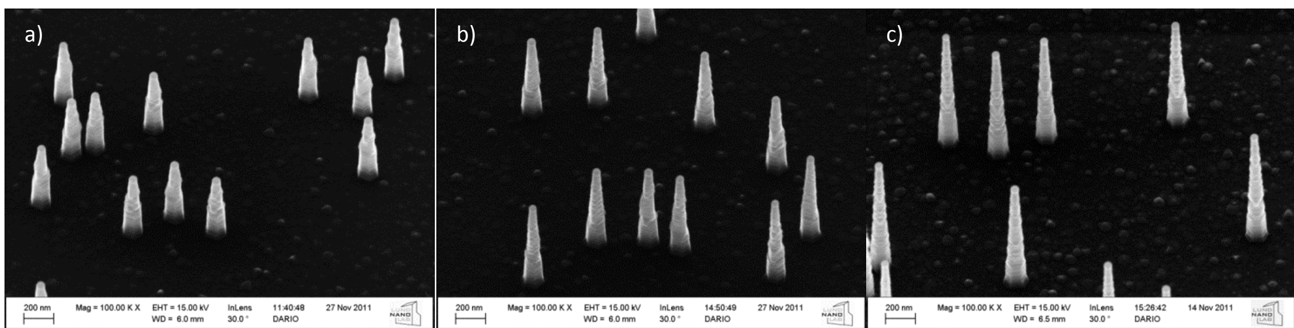

Figure B.3 Overview images of TMGa series at 100k magnification (a) #4836 (b) #4837 (c) #4838.

TMSb series	TMGa	Molar fraction	PH_3	Molar fraction	TMSb	Molar fraction	V/III	PH_3:TMSb
#4873	2/1000	8,07e-6	40	2,28e-3	8/1000	4,03e-5	287,3	49:1
#4874	2/1000	8,07e-6	40	2,28e-3	12/1000	6,04e-5	289,7	32,3:1
#4872	2/1000	8,07e-6	40	2,28e-3	16/1000	8,06e-5	292,2	27,6:1
#4673	2/1000	8,07e-6	40	2,28e-3	20/1000	1,01e-4	294,7	22,8:1

Table B.5 Growth parameters for TMSb series.

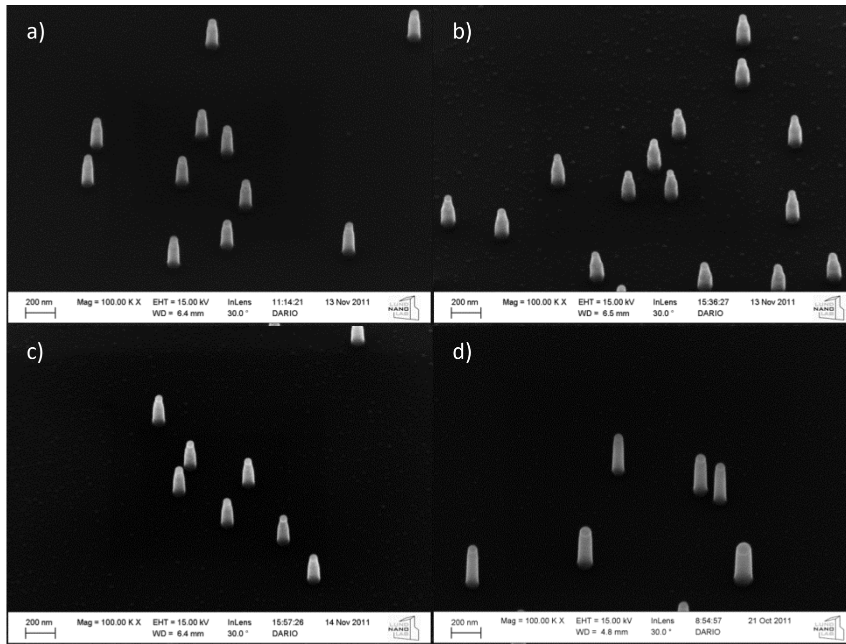

Figure B.4 Overview images of TMSb series at 100k magnification (a) #4873 (b) #4874 (c) #4875 (d) #4673.

Additional series	TMGa	Molar fraction	PH_3	Molar fraction	TMSb	Molar fraction	V/III	PH_3:TMSb
#5022	2/1000	8,07e-6	5	2,85e-4	20/300	3,36e-4	76,9	1:1,2
#5025	2/1000	8,07e-6	5	2,85e-4	8/300	1,34e-4	51,9	2,125:1
#5023	8/1000	3,23e-5	5	2,85e-4	20/300	3,36e-4	19,2	1:1,2
#5024	8/1000	3,23e-5	5	2,85e-4	8/300	1,34e-4	13	2,125:1

Table B.6 Growth parameters for the additional growth series.

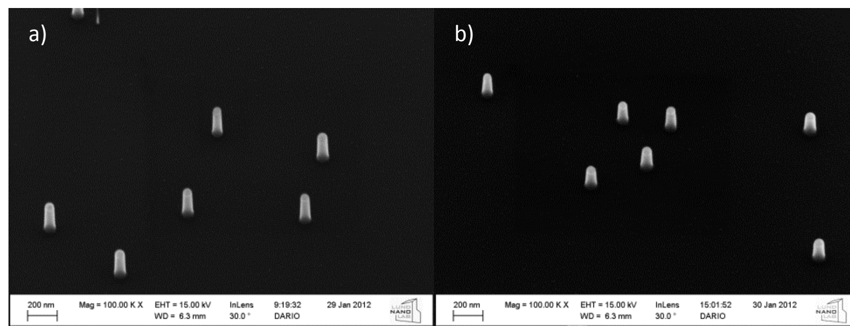

Figure B.5 Overview images of growth (a) #5022 (b) #5025 at 100k magnification.

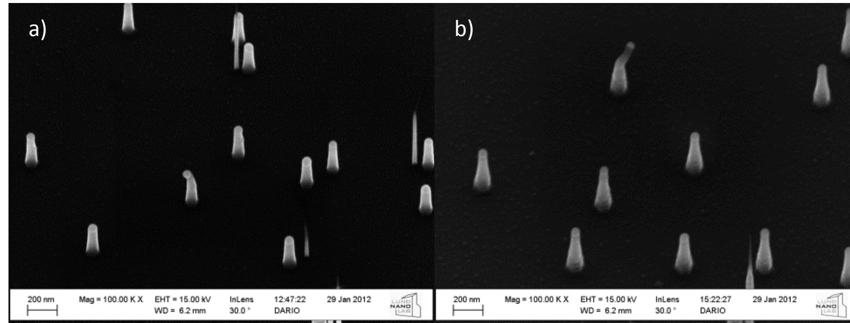

Figure B.6 Overview images of growth (a) #5023 (b) #5024at 100k magnification.

GaP/GaSb	TMGa	Molar fraction	PH_3	Molar fraction	TMSb	Molar fraction	V/III
#4675	2/1000	8,07e-6	40	2,28e-3	4,4/1000	2,22e-5	285

Table B.7 Growth parameters for GaP/GaSb. GaP stem for 2.5 min, transition from PH_3 to TMSb over 30s, GaSb for 15 min.

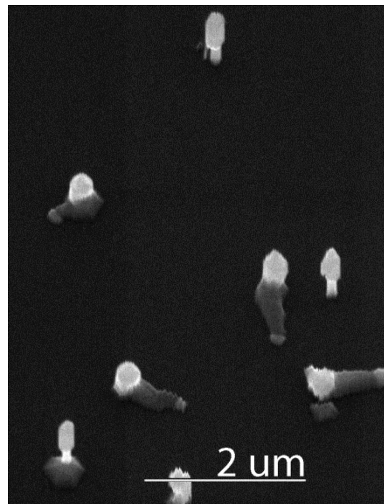

Figure B.7 GaP-GaSb heterostructure at 35k magnification.

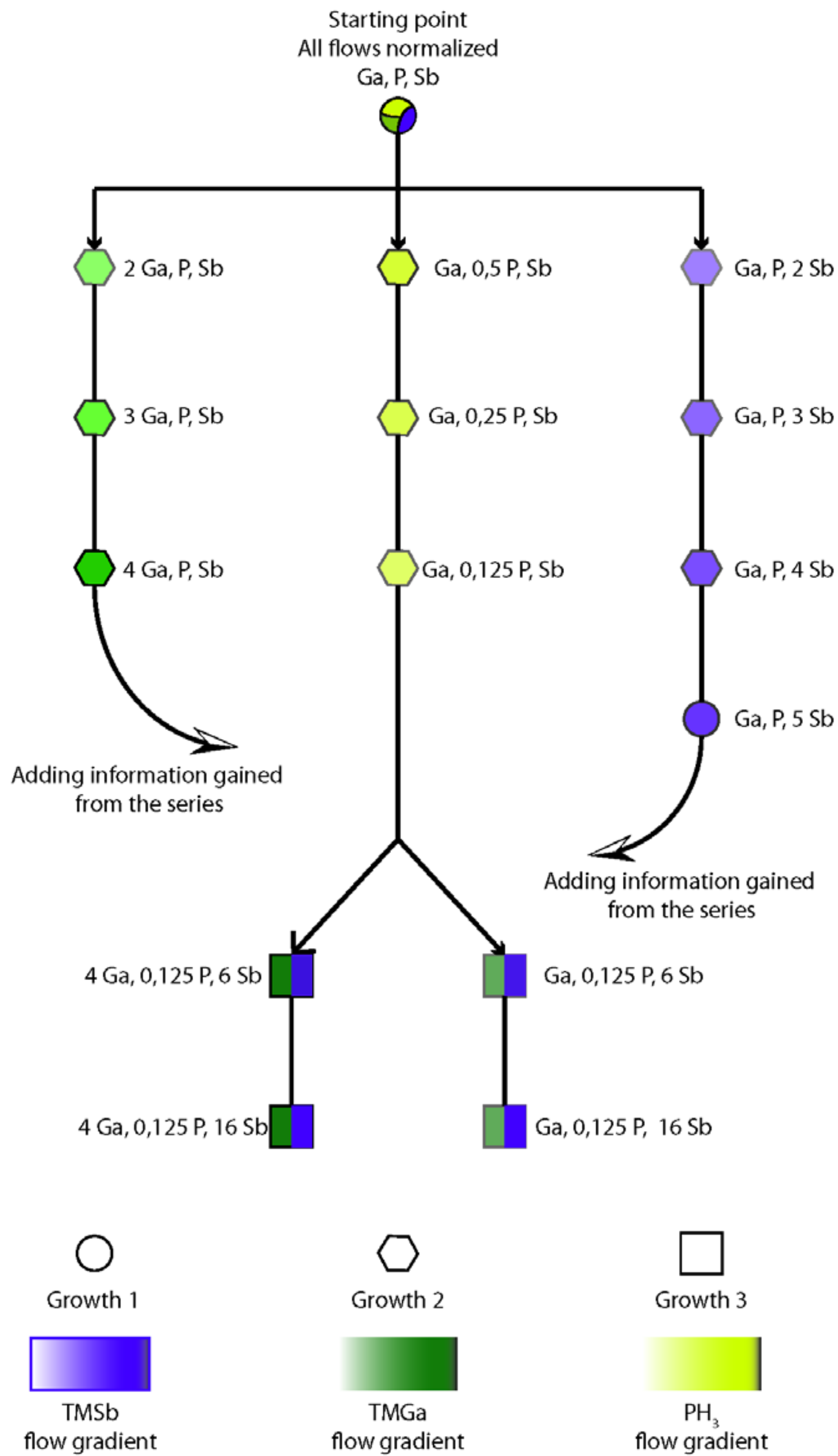

Figure B.8 Flow chart of growth experiments showing the relative molar fraction of the different sources.

Appendix B

EDS results

In this appendix typical EDS spectrums are shown to emphasize how the general spectrums for the Au particle and the ternary structure look like and to explain what is and can be seen from the spectrums. Tables with data from a few different nanowires on the samples analyzed with EDS are shown below. The tables will include data from the Au particle composition, the ternary region and for some nanowires the secondary Au particle. All data is shown in atomic% (at%) of the total composition of some selected interesting materials. The standard deviation of the detector is 1-2% requiring the user to check if it's a real value by examining the peaks of that material. For more information about the quantification method read "*Transmission Electron Microscopy*" by D. B. Williams and C.B. Carter [21 and refs within].

In all spectrums obtained during this project there are copper peaks from the grid on which the nanowires are placed on and a carbon peak from the carbon film holding the nanowires.

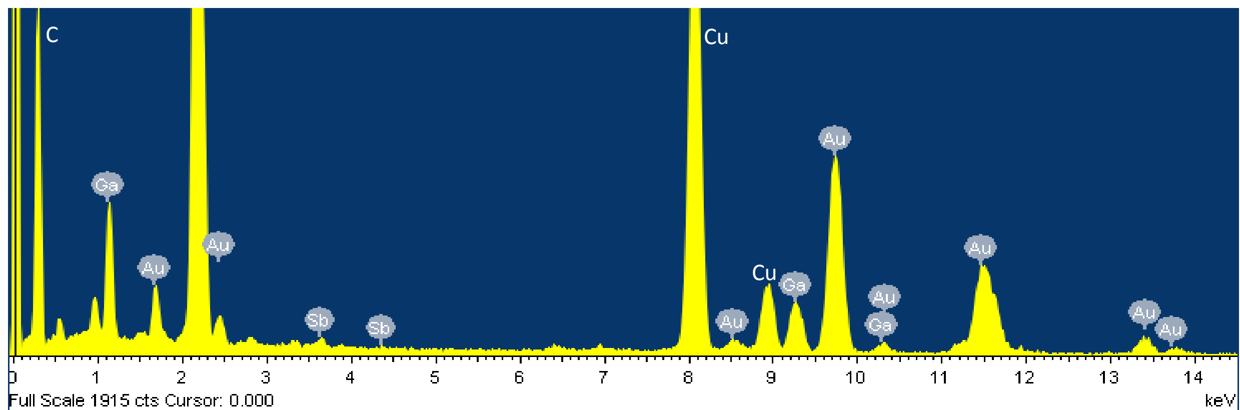

Figure C.1 A typical Au particle spectrum showing large Au and Ga peaks and minute Sb peaks.

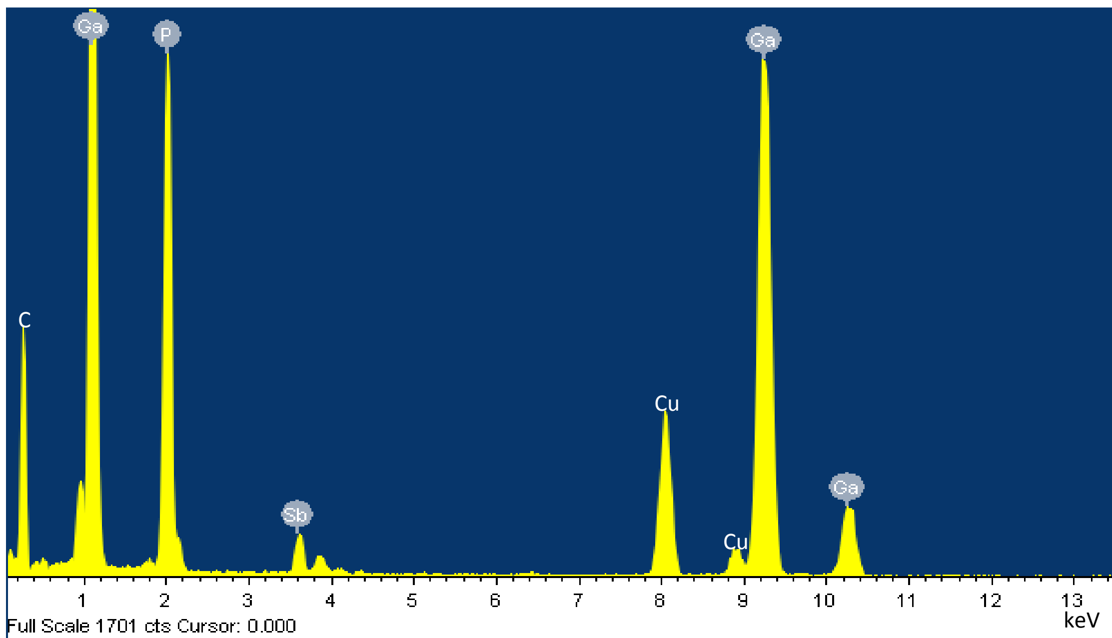

Figure C.2 A typical ternary spectrum showing the Ga and P peaks with a tiny amount of Sb.

Growth #4676, starting point					
Gold particle of nanowire #1					
Element	P	Ga	In	Sb	Au
At%	0,24	19,32	1,38	1,93	77,13
Ternary segment of nanowire #1					
Element	P	Ga	In	Sb	Au
At%	53,04	45,4	0	1,07	0,42
Gold particle of nanowire #2					
Element	P	Ga	In	Sb	Au
At%	1,34	18,73	1,26	0,74	77,94
Ternary segment of nanowire #2					
Element	P	Ga	In	Sb	Au
At%	50,58	46,91	0	2,02	0,41

Table C.1 Nanowires from starting point growth.

Growth #4834, end point of PH_3 series					
Gold particle nanowire #1					
Element	P	Ga	In	Sb	Au
At%	3,07	1,0	35,81	2,65	57,47
Ternary segment nanowire #1					
Element	P	Ga	In	Sb	Au
At%	59,57	36,76	0,47	2,86	0,34
Gold particle nanowire #2					
Element	P	Ga	In	Sb	Au
At%	1,24	1,56	38,3	2,07	56,82
Ternary segment nanowire #2					
Element	P	Ga	In	Sb	Au
At%	55,27	40,75	0,18	4,09	0

Table C.2 Nanowires from end point of PH_3 growth series.

Growth #4838, end point of TMGa series					
Gold particle nanowire #1					
Element	P	Ga	In	Sb	Au
At%	0,66	3,95	25,96	0,89	68,55
Ternary segment nanowire #1					
Element	P	Ga	In	Sb	Au
At%	59,56	38,61	0,21	1,5	0,12
Gold particle nanowire #2					
Element	P	Ga	In	Sb	Au
At%	0,71	4,17	26,13	1,11	67,86
Ternary segment nanowire #2					
Element	P	Ga	In	Sb	Au
At%	53,62	45,09	0	1,12	0,1

Table C.3 Nanowires from end point of TMGa growth series.

Growth #4872, end point TMSb series					
Gold particle nanowire #1					
Element	P	Ga	In	Sb	Au
At%	2,8	13,35	2,05	6,08	75,71
Ternary segment nanowire #1					
Element	P	Ga	In	Sb	Au
At%	57,63	41,16	0,03	1,00	0,18
Gold particle nanowire #2					
Element	P	Ga	In	Sb	Au
At%	0	13,79	4,5	1,07	80,87
Ternary segment nanowire #2					
Element	P	Ga	In	Sb	Au
At%	56,88	41,51	0	1,45	0,17
Gold particle nanowire #3					
Element	P	Ga	In	Sb	Au
At%	0,31	15,52	2,18	2,01	79,97
Ternary segment nanowire #3					
Element	P	Ga	In	Sb	Au
At%	58,46	39,9	0	1,43	0,39

Table C.4 Nanowires from end point of TMSb growth series.

Growth #5022, low TMGa, high TMSb					
Gold particle nanowire #1					
Element	P	Ga	In	Sb	Au
At%	0,47	14,21	6,73	0,49	78,09
Secondary gold particle nanowire #1					
Element	P	Ga	In	Sb	Au
At%	0,45	3,63	0,24	58,28	37,4
Ternary segment nanowire #1					
Element	P	Ga	In	Sb	Au
At%	54,95	42,83	0	1,91	0,22
Gold particle nanowire #2					
Element	P	Ga	In	Sb	Au
At%	1,01	12,47	7,33	0,62	78,57
Ternary segment nanowire #2					
Element	P	Ga	In	Sb	Au
At%	41,24	55,37	0	3,02	0,39
Gold particle nanowire #3					
Element	P	Ga	In	Sb	Au
At%	0	9,97	7,96	1,61	80,58
Ternary segment nanowire #3					
Element	P	Ga	In	Sb	Au
At%	49,81	47,17	0	2,52	0,44

Table C.5 Nanowires from low TMGa m.f. and high TMSb m.f. miniseries growth.

Growht #5025, low TMGa, medium TMSb					
Gold particle nanowire #1					
Element	P	Ga	In	Sb	Au
At%	0,76	13,75	1,77	4,37	79,35
Ternary segment nanowire #1					
Element	P	Ga	In	Sb	Au
At%	58,09	39,88	0	1,74	0,29
Gold particle nanowire #2					
Element	P	Ga	In	Sb	Au
At%	0,76	16,12	1,6	2,44	79,08
Ternary segment nanowire #2					
Element	P	Ga	In	Sb	Au
At%	47,19	49,96	0	2,48	0,38

Table C.6 Nanowires from low TMGa m.f. and medium TMSb m.f. miniseries growth.

Growth #5023, high TMGa, high TMSb					
Gold particle nanowire #1					
Element	P	Ga	In	Sb	Au
At%	2,34	25,55	0	4,85	67,26
Ternary segment nanowire #1					
Element	P	Ga	In	Sb	Au
At%	43,87	53,58	0	2,11	0,43
Gold particle nanowire #2					
Element	P	Ga	In	Sb	Au
At%	0,46	15,69	0	0,62	83,23
Ternary segment nanowire #2					
Element	P	Ga	In	Sb	Au
At%	51,03	44,47	0	3,95	0,55
Gold particle nanowire #3					
Element	P	Ga	In	Sb	Au
At%	0	15,63	4,44	0,27	79,93
Secondary gold particle nanowire #3					
Element	P	Ga	In	Sb	Au
At%	0,32	2,79	0,3	59,79	36,8
Ternary segment nanowire #3					
Element	P	Ga	In	Sb	Au
At%	48,16	50,08	0	1,46	0,24

Table C.7 Nanowires from high TMGa m.f. and high TMSb m.f. miniseries growth.

Growth #5024, high TMGa, medium TMSb					
Gold particle nanowire #1					
Element	P	Ga	In	Sb	Au
At%	0,93	12,1	5,82	2,35	78,8
Secondary gold particle nanowire #1					
Element	P	Ga	In	Sb	Au
At%	8,67	1,03	0	59,93	31,24
Ternary segment nanowire #1					
Element	P	Ga	In	Sb	Au
At%	49,26	46,42	0,2	3,71	0,4
Gold particle nanowire #2					
Element	P	Ga	In	Sb	Au
At%	0	15,05	3,77	0,81	80,41
Ternary segment nanowire #2					
Element	P	Ga	In	Sb	Au
At%	43,93	52,82	0	2,99	0,29

Table C.8 Nanowires from high TMGa m.f. and medium TMSb m.f. miniseries growth.

References

[1] E.K. Müller, J.L. Richards, “*Miscibility of III-V Semiconductors Studied by Flash Evaporation*”, J. Appl. Phys., **35**(4) (1964) pp. 1233-1241

[2] G.B. Stringfellow, “*Calculation of Ternary Phase Diagrams of III-V Systems*”, J. Phys.Chem. Solids **33** (1972) pp. 665-677

[3] G.B. Stringfellow, “*Calculation of Ternary and Quaternary III-V Phase Diagrams*”, J. Cryst. Growth **27** (1974) pp. 21-34

[4] K. Ishida, T. Nomura, H. Tokunaga, H. Ohtani, T. Nishizawa, “*Miscibility gaps in the GaP-InP, GaP-GaSb, InP-InSb and InAs-InSb systems*”, Journal of Less-Common Metals **155** (1989), pp. 193-206

[5] M.R. Leys, M.E. Pistol, H. Titze, L. Samuelson, “*On the growth of gallium phosphide layers on gallium phosphide substrates by MOVPE*”, J. Elec. Mat. Vol. **18** issue. **1** (1989) pp. 25-31

[6] H. Ibach, H. Lüth, “*Solid-State Physics. An introduction to Principles of Material Science*”, 3rd ed., Springer-Verlag, Berlin Heidelberg, Germany, 2003

[7] P. Caroff, J. Bolinsson, J. Johansson, “*Crystal Phases in III-V Nanowires: From Random Toward Engineered Polytypism*”, JSTQE vol. **17** issue. **4** (2010) pp. 829-846

[8] L. Vegard, “*Die Konstitution det Mischkristalle und die Raumfüllung der Atome*”, Zeitschrift für Physik, Julius Springer, Berlin (1921)

[9] C.A. Larsen, G.B. Stringfellow, “*Decomposition kinetics of OMVPE precursors*”, J. Crystal Growth **75** (1986) pp. 247-254

[10] G.B. Stringfellow “*Thermodynamic aspects of OMVPE*”, J. Cryst. Growth **70** (1984) pp. 133-139

[11] G.B. Stringfellow, “*Organometallix Vapor-Phase Epixaty*”, Academic Press, Boston, MA, 1989

[12] D.L. Smith, “*Thin-film deposition: principles and practice*”, McGraw Hill, inc., 1995

[13] I. V. Makrov, “*Crystal growth for beginners*“, World Science Publishing Co., Singapore, 2003

[14] C. Soci, X. Y. Bao, D.P.R. Aplin, D. Wang, “*A Systematic Study on the Growth of GaAs Nanowires by Metal-Organic Chemical Vapor Deposition*”, Nano Lett. vol. **8** no. **12** (2008) pp. 4275-4282

[15] H.M. Manasevit, W.I. Simpson “*The Use of Metal-Organics in the Preparation of Semiconductor Materials, I. Epitaxial Gallium-V Compounds*”, J. Electrochem. Soc **116** (1969) pp. 1725-1732

[16] R. Lückerath, P. Tommack, A. Hertling, H. J. Koss, P. Balk, K. F. Jensen, W. Richter, ”*CARS in situ diagnosticsin MOVPE: the thermal decomposition of AsH_3 and PH_3*”, J. Cryst. Growth **93** (1988), pp. 151-158

[17] S. P. Den Baars, B. Y. Maa, P. D. Dapkus, A. D. Danner, H. C. Lee, ”*Homogeneous and heterogeneous thermal decomposition rates of trimethylgallium and arsine and their relevance to the growth of GaAs by MOCVD*”, J. Cryst. Growth **77** (1986), pp. 188-193

[18] H. J. Joyce, Y. Kim, Q. Gao, H. H. Tan, C. Jagadish, “*Optimised Two-Temperature Growth of GaAs Nanowires by Metalorganic Chemical Vapour Deposition*”, COMMAD (2006), pp. 172-175

[19] J. Wallentin, M. E. Messing, E. Trygg, L. Samuelson, K. Deppert, M. T. Borgström, ”*Growth of doped $InAs_yP_{1-y}$ nanowires with InP shells*“, J. Cryst. Growth **331** (2011), pp. 8-14

[20] K. A. Dick, S. Kodambaka, M. C. Reuter, K. Deppert, L. Samuelson, W. Seifert, L. R. Wallenberg, F. M. Ross, “*The Morphology of Axial and Branched Nanowire Heterostructures*”, Nano Lett. vol. **7** no. **6** (2007), pp. 1817-1822

[21] D.B. Williams, C.B. Carter, “*Transmission Electron Microscopy*”, Springer-Verlag, New York, NY, 2009

[22] Oxford Instruments: X-ray Energy Dispersive Spectroscopy (EDS) detector, http://www.oxford-instruments.com/Campaigns/microanalysis/eds/Pages/eds-system.aspx

[23] Vul' A.Ya., M. Levinshtein, S. Rumyantsev and M. Shur “*Handbook Series on Semiconductor Parameters”*, **vol.1**, World Scientific, London, 1996

[24] H. Landolt, R. Börnstein “*Landolt-Börnstein: Numerical Data and Functional Relationships in Science and Technology - New Series*”, Springer Science and Business Media

[25] R.M. Beifeld, “*The metal-organic chemical vapor deposition and properties of III-V antimony-based semiconductor material*”, Materials Science and Engineering **R 36** (2002) pp. 105-142

[26] C.M. Fetzer, R.T. Lee, G.B. Stringfellow, “*Effect of surfactant Sb on carrier lifetime in GaInP epilayer*”, J. App. Phys. **91** (2002) 199

[27] C.A. Larsen, S.H. Li, G.B. Stringfellow, “*Decomposition Mechanisms of Trimethylantimony and Reactions with Trimethylindium*”, Chem. Mater. **3** (1991) pp. 39-44

[28] P. Caroff, J. B. Wagner, K. A. Dick, H. A. Nilsson, M. Jeppsson, K. Deppert, L. Samuelson, L. R. Wallenberg, L-E Wernersson, “*High-Quality InAs/InSb Nanowire Heterostructures Grown by Metal–Organic Vapor-Phase Epitaxy*”, small vol. **4** no. **7** (2008) pp. 878-882

[29] S. Loualiche, A. Le Corre, S. Salaun, J. Caulet, B. Lambert, “*GaPSb: A new ternary material for Schottky diode fabrication on InP*”, Appl. Phys. Lett. **59** (1991) 423

[30] M.J. Jou, G.B. Stringfellow, “*Organometallic vapor phase epitaxy of GaPSb and InPSb*”, J. Crystal Growth **98** (1989) pp. 679-689

[31] A.D. Howard, D.C. Chapman, G.B. Stringfellow, "*Effects of surfactant Sb and Bi on incorporation of zinc and carbon in III/V materials grown by organometallic vapor phase epitaxy*", J. App. Phys. **100** (2006) 044904

[32] M. Jeppson, K.A. Dick, J.B. Wagner, P. Caroff, K. Deppert, L. Samuelson, L-E. Wernersson "*GaAs/GaSb nanowire heterostructures grown by MOVPE*", J. Crystal Growth **310** (2008) pp. 4115-4121

[33] M. Jeppson, K.A. Dick, H. A. Nilsson, N. Sköld, J.B. Wagner, P. Caroff, L-E. Wernersson "*Characterization of GaSb nanowires grown by MOVPE*", J. Crystal Growth **310** (2008) pp. 5119-5122

[34] R.T. Lee, J.K. Shurtleff, C.M. Fetzer, G.B. Stringfellow, S. Lee, "*Surfactant controlled growth of GaInP by organometallic vapor phase epitaxy*", J. App. Phys. **87** (2000) 3730

[35] T. Xu, K.A. Dick, S. Plissard, T.H. Nguyen, Y. Makoudi, M. Berthe, J-P. Nys, X. Wallart, B. Grandidier, P. Caroff *"Faceting, composition and crystal phase evolution in III–V antimonide nanowire heterostructures revealed by combining microscopy techniques*", Nanotechnology **23** (2012) 095702

[36] M.J. Jou, Y.T. Cherng, H.R. Jen, G.B. Stringfellow, "*OMVPE growth of the new semiconductor alloys* $GaP_{1-x}Sb_x$ *and* $InP_{1-x}Sb_x$", J. Crystal Growth **93** (1988) pp. 62-69

[37] M.J. Jou, G.B. Stringfellow, "*Organometallic vapor phase epitaxial growth studies of* $GaP_{1-x}Sb_x$ *and* $InP_{1-x}Sb_x$", J. Crystal Growth **98** (1989) pp. 679-689

[38] P. Caroff, M. E. Messing, B. M. Borg, K. A. Dick, K. Deppert, L-E. Wernersson, "*InSb heterostructure nanowires: MOVPE growth under extreme lattice mismatch*" Nanotechnology **20** (2009) 495606

[39] G.B. Stringfellow, "*OMVPE growth of* $GaAs_xSb_{1-x}$ *: solid composition*", J. Cryst. Growth **64** (1983) pp. 413-415

[40] Y.N. Guo, J. Zou, M. Paladugu, H. Wang, Q. Gao, H.H. Tan, C. Jagadish, "*Structural characteristics of GaSb/GaAs nanowire heterostructures grown by metal-organic chemical vapor deposition*", Appl. Phys. Lett. **89** (2006) 231917

[41] R. M. Biefeld, "*The metal-organic chemical vapor deposition and properties of III-V antimony-based semiconductor materials*", Materials Science and Engineering R **36** (2002), pp. 105-142

[42] B. M. Borg, K. A. Dick, J. Eymery, L-E. Wernersson, "*Enhanced Sb incorporation in InAsSb nanowires grown by metalorganic vapor phase epitaxy*", App. Phys. Lett. **98** (2011), 113104

[43] H. Zhou, M. Pozuelo, R. F. Hicks, S. Kodambaka, "*Self-catalyzed vapor-liquid-solid growth of InP_xSb_{1-x} nanostructures*", J. Cryst. Growth **319** (2011), pp. 25-30

[44] M. Borg, "*Antimonide Heterostructure Nanowires – Growth, Physics and Devices*", Media-Tryck, Lund, 2012

[45] John Emsley, "*The Elements 3th edition*", Oxford University Press, Oxford UK, 1999

[46] V.G. Dubrovskii, N.V. Sibirev, J.C. Harmand, F. Glas, "*Growth kinetics and crystal structure of semiconductor nanowires*", Phys. Rev. B **78** (2008), 235301

[47] J. Johansson, L.S. Karlsson, K. A. Dick, J. Bolinsson, B.A. Wacaser, K. Deppert, L. Samuelson, "*Effects of Supersaturation on the Crystal Structure of Gold Seeded III-V Nanowires*", Cryst. Growth Des., **9** (2), (2009) pp. 766–773

[48] G.B. Stringfellow, "*Novel precursors for organometallic vapor phase epitaxy*", J. Crystal Growth **128** (1993) pp. 503-510

[49] R.D. Dupuis "*Metalorganic Chemical Vapor Deposition of III-V Semiconductors*", Science vol. **226**, no. **4675** (1984) pp. 623-629

[50] H.M. Manasevit "*Recollections and reflections of MO-CVD*", J. Cryst. Growth **55** (1981) pp. 1-9

[51] M. Messing, "*Engineered Nanoparticles Generation, Characterization and Applications*", Media-Tryck, Lund, 2011

[52] J. Bolinsson, "*The Crystal Structure of III-V Semiconductor Nanowires: Growth and Characterization*", Media-Tryck, Lund, 2010

[53] G.B. Stringfellow, "*A critical appraisal of growth mechanisms in MOVPE*", J. Cryst. Growth **68** (1984) pp. 111-122

[54] J. Johansson, C. P. T. Svensson, T. Mårtensson, L. Samuelson, W. Seifert "*Mass Transport Model for Semiconductor Nanowire Growth*", J. Phys. Chem. B **109** (2005), pp. 13567-13571